Ammonia Fuelled Solid Oxide Fuel Cell to Power Maritime Applications

KRISTOFFER HJARTHOLM KALSTAD

SUPERVISORS
Peter Hugh Middleton
Gunstein Skomedal

University of Agder, 2021
Faculty of Engineering and Science
Department of Engineering Sciences

Abstract

Ammonia fuelled solid oxide fuel cell (SOFC) systems are regarded as a promising alternative-for energy production due to high efficiency and low environmental impact. Ammonia is a carbon free compound with high energy density, low production cost and much simpler transport- and storage properties than hydrogen. The state-of-the-art SOFC contains a Ni/YSZ anode which has proven to be an effective catalyst to crack ammonia at intermediate temperatures (~700°C). In this study an experimental work was conducted using an Open Flange SOFC test set-up with a planar anode-supported single cell consisting of a Ni/YSZ anode, YSZ electrolyte, and LSM cathode. The objective of the study is to investigate the feasibility of using vaporised ammonia solution as fuel in SOFC systems. For safety reasons the experimental supply of ammonia was from an aqueous solution of 32wt%. The experiments were divided into two parts. In the first part three variations of ammonia concentration (32wt%, 15.2wt% and 5.9wt%) were supplied to the fuel cell to investigate the current – voltage behaviour obtained at 750 ^{0}C. Maximum power densities at 45 mW/cm^2, 37.5 mW/cm^2, and 25 mW/cm^2 respectively were observed which were consistent with the reduction in partial pressure and mass flow of ammonia as the concentration of ammonia in the aqueous solution was decreased. The second part of the experiment was a comparison of 32wt% ammonia solution with pure hydrogen and a 3:1 hydrogen/nitrogen mixture. It was observed that the maximum power densities of the 32%wt ammonia solution reached power densities comparable to the ones obtained with hydrogen as fuel at 850°C.

Preface

This report acts as the final step of fulfilling my master's program of Renewable Energy at the Faculty of Engineering and Science, University of Agder Campus Grimstad. The project period lasted from January to May 2021 with the purpose of build a test-station and test an Open Flange SOFC fuelled by ammonia.

I would like to thank my supervisor Peter Hugh Middleton for sharing some of his invaluable expertise and experience of conducting a fuel cell experiment. I am also grateful for all the helpful advice and feedback provided by Gunstein Skomedal throughout the entirety of the project. At last, I would like to express my appreciation to the lab manager Odin Kvam for showing his interest in the project and to help with significant improvements of the lab facilities.

Individual/group Mandatory Declaration

The individual student or group of students is responsible for the use of legal tools, guidelines for using these and rules on source usage. The statement will make the students aware of their responsibilities and the consequences of cheating. Missing statement does not release students from their responsibility.

1.	I/We hereby declare that my/our report is my/our own work and that I/We have not used any other sources or have received any other help than mentioned in the thesis.	☒
2.	I/we further declare that this thesis: - has not been used for another exam at another department/university/university college in Norway or abroad; - does not refer to the work of others without it being stated; - does not refer to own previous work without it being stated; - have all the references given in the literature list; - is not a copy, duplicate or copy of another's work or manuscript.	☒
3.	I/we am/are aware that violation of the above is regarded as cheating and may result in cancellation of exams and exclusion from universities and colleges in Norway, see Universitets- og høgskoleloven §§4-7 og 4-8 og Forskrift om eksamen §§ 31.	☒
4.	I/we am/are aware that all submitted theses may be checked for plagiarism.	☒
5.	I/we am/are aware that the University of Agder will deal with all cases where there is suspicion of cheating according to the university's guidelines for dealing with cases of cheating.	☒
6.	I/we have incorporated the rules and guidelines in the use of sources and references on the library's web pages.	☒

Publishing Agreement

Authorization for electronic publishing of the thesis.

Author(s) have copyrights of the thesis. This means, among other things, the exclusive right to make the work available to the general public (Åndsverkloven. §2).

All theses that fulfill the criteria will be registered and published in Brage Aura and on UiA's web pages with author's approval.

Theses that are not public or are confidential will not be published.

I hereby give the University of Agder a free right to

make the task available for electronic publishing: ☒JA ☐NEI

Is the thesis confidential? ☐JA ☒NEI

(confidential agreement must be completed and signed by the Head of the Department)

- If yes:

Can the thesis be published when the confidentiality period is over? ☐JA ☐NEI

Is the task except for public disclosure? ☐JA ☐NEI

(contains confidential information. see Offl. §13/Fvl. §13)

Table of Contents

List of Figures

List of Tables

Notation

A	Area of cell
a	Activity
C	Capacitance
E	Reversible Voltage
F	Faradays Constant
i	Current
j	Current Density
L	Inductance
i_0	Exchange Current Density
P_X	Partial pressure of species X
P	Standard Pressure
R	Universal Gas Constant
Z	Impedance
Y	Admittance

Greek Letters

α	Transfer Coefficient
τ	Thickness (anode, cathode, electrolyte
σ	Conductivity
ω	Angle Frequency
ΔH	Enthalpy
ΔS	Entropy
ΔG	Gibbs Free Energy
V	Voltage
η_{act}	Activation loss
η_{con}	Concentration loss
η_{ohm}	Ohmic loss
ΔC	Heat Capacity

Abbreviations

AER	Annual Efficiency Ratio
CCS	Carbon Storage and Capture
EEOI	Energy Efficiency Operational Index
GHG	Greenhouse Gas
H_2	Hydrogen
HB	Haber Bosch
HCC	Heat Capacity Coefficient
HCF	Heat Capacity Factor
ICE	Internal Combustion Engine
IMO	International Maritime Organisation
IT	Intermediate Temperature
LNG	Liquid Natural Gas
LT	Low Temperature
MGO	Marine Gasoil
N_2	Nitrogen
NH_3	Ammonia
Ni	Nickel
PEM	Proton Exchange Membrane
SOFC	Solid Oxide Fuel Cell
SR	Steam Reforming
YSZ	Yttria Stabilised Zirconia

1 Introduction

Fuelling solid oxide fuel cell (SOFC) systems with ammonia is one of the most promising alternatives of producing environmentally friendly and efficient energy in the maritime sector. One of the biggest obstacles of hydrogen are high cost due to complex storage- and transport properties and low volumetric density but is both very well handled by storing hydrogen in ammonia. Ammonia is a carbon free fuel that liquified at moderate temperatures and pressures and has already an existing global infrastructure. SOFC is regarded a leader among clean power production technologies due to its high efficiency and capability to utilise alternative fuels such as hydrocarbons and ammonia. The state-of-the-art SOFC is composed a Ni/YSZ anode which has proven to be an effective catalyst to crack ammonia at typical operating temperature. This report presents a master's thesis investigating the feasibility of ammonia as fuel in SOFC. A lab experiment of an Open Flange SOFC was conducted, and an electrochemical model was developed. This chapter presents the emissions and targeted cuts in the Maritime sector set by the International Maritime Organisation (IMO) and an introduction to ammonia and fuel cells. The two latter topics are further explained in chapter 2.

1.1 Maritime Sector

There is a broad agreement among scientists that the global greenhouse gas (GHG) emission is causing an increased global average temperature. To prevent dramatic consequences the United Nations (UN) stated that reductions of global GHG emissions must reach 50% by 2030 and close to net-zero by 2050 compared to pre-industrial emissions[1]. The maritime sector was in 2018 responsible for approximate 2.89% of the total global emissions, corresponding to 1.056 million tonnes of CO_2 annually[2]. Until 2018, the maritime sector was without evident regulations of GHG emissions, and the transition towards relative expansive and undeveloped sustainable fuels has been hold back. In line with the Paris Agreement the IMO, an agency of UN who are responsible for environmental regulations in the maritime sector among other things, adopted in April 2018 an initial strategy with the ambition:

> *"to peak GHG emissions from international shipping as soon as possible and to reduce the total annual GHG emissions by at least 50% by 2050 compared to 2008 whilst pursuing efforts towards phasing them out as called for in the Vision as a point on a pathway of CO2 emissions reduction consistent with the Paris Agreement temperature goals*[3]*".*

Development of sustainable fuels and associated power generation technologies to an extent where they can compete, or even surpass, the fossils fuels will be crucial if the targeted emissions cuts shall be reached. To fulfil the ambitions is short-, mid-, and long-term implementation of regulations planned, displayed in table 1[4].

Table 1: Short-, mid-, and long term GHG reduction measures in the maritime sector[4].

Periods	2018-2023	2023-2030	2030-2050
GHG reductions measures	- Improve energy efficiency framework - Develop technical and operational energy efficiency measures - Encourage national policies, incentives, and port activities - Undertake additional GHG emission studies	- Implement *for the effective uptake of alternative fuel* - Operational energy efficiency measures - Innovative emission reduction mechanism - Enhance technical cooperation - Develop feedback mechanism to learn and share information	- Pursue the development and provision of alternative fuels - Encourage and facilitate the general adoption of other possible innovative emission reduction mechanism

1.1.2 Transport and emissions

From 1990 to 2008, there was an equal rate of growth in demand and CO_2 emissions in the maritime sector as seen in Fig 1[2]. Significant improvements in carbon intensity (Annual Efficiency Ratio (AER) and Energy Efficiency Operational Index (EEOI)) resulted in 2008 in a negative trend of CO_2 emissions in the maritime sector, even with a continuous increase in demand. The reductions continued until around 2014 where the growth of demand surpassed the moderate EEIO and AER improvements, and the emissions started to slightly increase again. IMO predicts in their fourth IMO GHG Study from 2020 [2] an increase of CO_2 emissions by 0 to 500 million tonnes annually from 2018 to 2050 for numerous scenarios without the implementation of regulations impacting the emissions. Fig 2 displays their predictions for various socio economics- and energy scenarios[2].

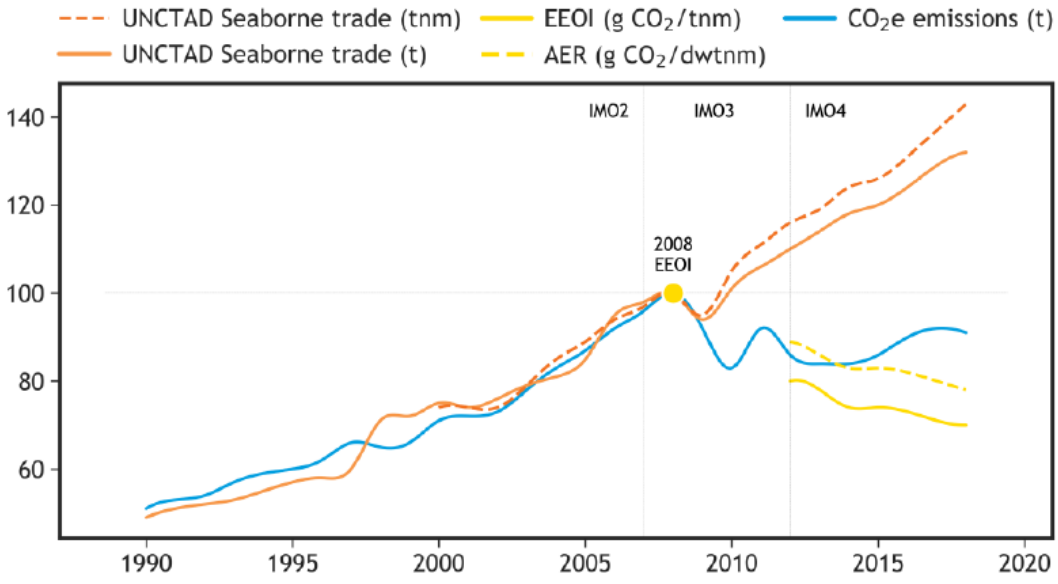

Figure 1: CO2 emissions and trade demand from 1990-2018[2]

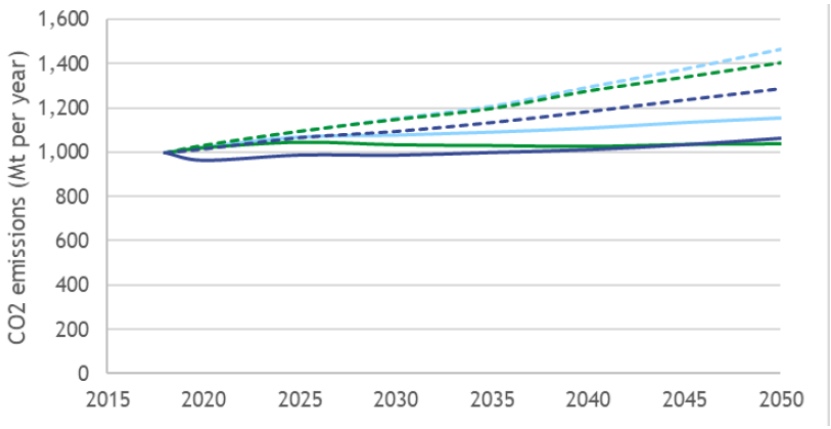

Figure 2 Predicted missions in the years to come without implementation of regulations[2]

1.1.3 Pathway ahead

So far, the biggest portion of GHG reduction is obtained through energy efficiency improvements such as ship design, lighter materials, and waste heat recovery. However, going further to implement carbon-neutral fuels in the maritime sector is essential to achieve IMOs 2050 target. DNV GL released in 2020 a case study of a Panamax bulk carrier forecasting the implementation weight of sustainable fuels for 30 scenarios in three decarbonation ambitions or pathways[5]:

1. ***No ambitions*** – pathway without further decarbonization regulations.
2. ***IMOs ambitions*** – pathway following IMOs initial strategy.
3. ***Decarbonization by 2040*** – pathway where stakeholder apply pressure on the industry resulting in IMO to upward their ambitions.

DNV GL presented an ambitious scenario where pressure from stakeholder enhances the growth rate of carbon neutral fuels in the maritime sector. As seen in Fig 3, the share of carbon-neutral fuel could reach 35% by 2030 and 100% by 2040, meaning the shift is happening during the lifetime of the vessels built today. Because of the immaturity of the present ammonia fuelled power generation and associated safety issues, the vessels in the *Decarbonization by 2040* scenario are built to run on one fuel and transfer to carbon-neutral fuel during their lifetime[5]. Because of the maturity of the technologies, it is expected that ammonia as fuel will first be implemented in ships will modified ICE systems to utilise it as fuel, while SOFC acts more as a support system[5][6].

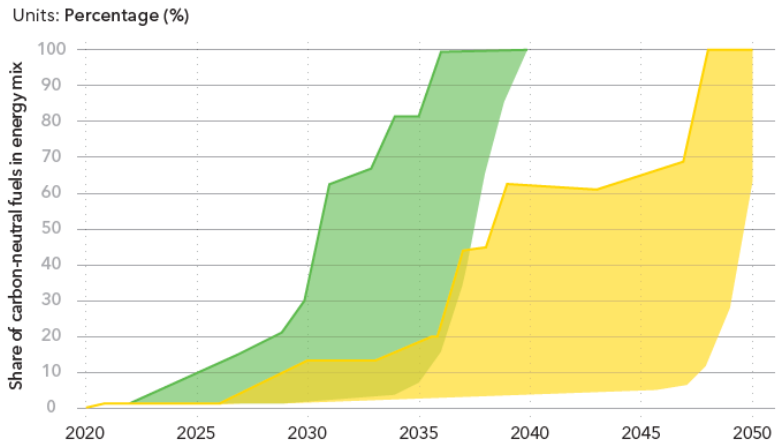

Figure 3: Share of carbon-neutral fuel in the maritime sector for IMOs 2050 and 'Decarbonization by 2040' strategy [5]

1.2 Ammonia as Sustainable Fuel

Using hydrogen stored in ammonia is a beneficial method of fuelling zero-emission power generation in the maritime sector. Ammonia is a compound of nitrogen and hydrogen that has been commercial produced since the ammonia synthesis, also known as the Haber Bosch (HB) process, was invented by Fritz Haber and Carl Bosch in the early 20th century. Besides being completely carbon free, it liquifies at moderate pressures and temperatures, and has a higher volumetric energy density than hydrogen. It has already been traded on a global scale for decades and in 2018 the global production of ammonia was approximate 176 million tonnes[7], meaning the global infrastructure is already in place.

Obstacles of high GHG emission during production needs solving prior to considering ammonia as a sustainable fuel. The production of ammonia is a very energy intensive process standing for around 1.8% of the global energy demand, mainly due to the steam reforming (SR) of hydrocarbons to produce the hydrogen (H_2) supplied to the ammonia synthesis. SR of hydrogen is responsible for around 500 million tonnes of annual carbon dioxide emission and 80% of the total ammonia production energy consumption[7], meaning decarbonation of the hydrogen production is crucial if ammonia shall be considered a sustainable fuel. The planning of electrolysis has developed quickly recent years and there is predicted a significant growth it the years to come. This topic is further elaborated in chapter 2.

1.3 Fuel Cells

Fuel cells is regarded a clean source of energy with high electrical efficiencies typically found between 40-60%[8]. They function by supplying hydrogen holding fuels to an electrochemical process that converts chemical energy stored in hydrogen into electrical energy, with the potential of water being the only biproduct.

1.3.1 Working Principle

A fuel cell is composed by two electrodes (anode and cathode) with an electrolyte sandwiched in between. The working principles are similar the ones of batteries but are differentiated by the demand of a continuous supply of fuel during operation. The chemical reactions of the perhaps most conventional fuel cell, the Proton Exchange Membrane (PEM), are presented in Fig 4. Hydrogen is supplied to the anode and is oxidated over a catalyst, forming hydrogen ion (H^+) and free electrons (e^-). The electrons are passing through an external circuit while the ions are conducted through the ion-conducting electrolyte. Oxygen or air is supplied to the cathode which reacts with the hydrogen and electrons to form water. SOFC is usually composed by an oxide-conducting electrolyte which results is slightly different path of reaction, and if further elaborated in chapter 2.3.

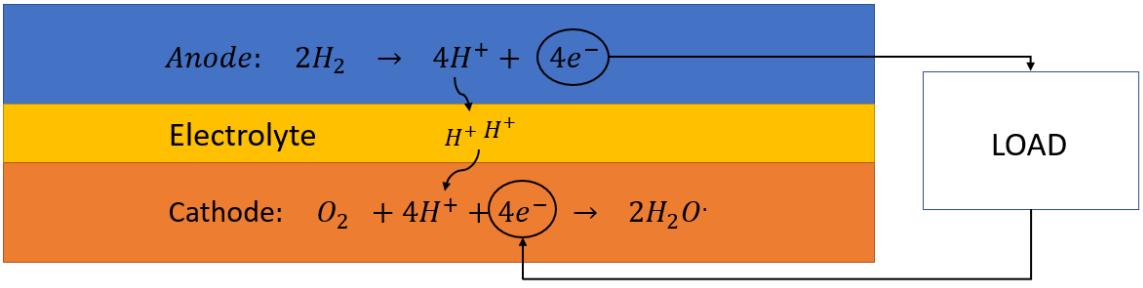

Figure 4: Schematic of a conventional PEM fuel cell

1.3.2 Comparison of fuel cell

There are five main types of fuel cell found in literatures: Polymer Electrolyte Membrane (PEM), Alkaline (AFC), Phosphoric Acid (PAFC), Molten Carbonate (MCFC) and Solid Oxide (SOFC). The working principles are similar for all of them, but the electrolyte (which they are named by) dictates certain properties such as operational temperature and fuel compatibility. A collection of typical materials, temperatures and efficiencies for the mentioned fuel cells are given in table 2.

Table 2 Collection fuel cells and typical materials, operating temperature and efficiency [8]

Fuel Cell Type	Material and Catalyst	Electrolyte	Operating Temperature [°C]	Efficiency [%]
SOFC	Ceramic and Pervoskites	Ceramics (YSZ)	500-1000	50-60
PEM	Carbon and Pervoskites	Solid Membrane (nafion)	30-100	40-50
Direct Methanol FC	Platinum and Ruthenium	Solid Membrane	20-90	20-50
Alkaline FC	Carbon and Nickel	Potassium hydroxide	20-300	50-60
Molten Carbonated FC	Stainless steel and Nickel	Carbonated Metal	~650	>60

1.3 Ammonia in Solid Oxide Fuel Cells

Fuelling SOFC with ammonia is a novel method of power generating that has an increased rate of interest the last few decades. SOFC is regarded as a leader among power generation systems in terms of conversion efficiency, fuel flexibility and environmental impact[9], and has great potential of becoming a viable option of producing clean and efficient energy, perhaps two of the most important traits in the futuristic energy production marked. High reactions rates can be achieved without the need of rare catalysts materials and it is capable of internal reforming thanks to its high operating temperatures (~800) [8]. This also gives the opportunity of using fuels such as hydrocarbons and ammonia without external reforming- or cracking units, reducing cost and need of free area while also avoiding the complexity of handling with pure hydrogen. Hydrocarbons has advantages of availability and low cost, but results in emission of GHG and nickel SOFC anodes are often made of nickel which is victim of degradation due to the formation of coke[10].

The issues associated with complex handling of hydrogen as well as the mentioned problems of using hydrocarbons are solved by ammonia, and nickel has proven to be an excellent catalyst for the ammonia cracking process. Several studies have shown close to equally good results of ammonia and hydrogen in SOFC systems[10], [11], [12], [13]. It is difficult to identify obvious downsides of ammonia as fuel in SOFC, but providing clean hydrogen to the ammonia synthesis, handling of safety due to its toxicity, and improve the general applicability of SOFC to a commercial level are obstacles that need attention.

1.4 Research Questions

The general objective of this master's thesis is to investigate the performance of SOFC fuelled my ammonia, with focus on the applicability in the maritime sector. The research question that needs answering can be compressed as:

"Can SOFC fuelled by ammonia become a feasible alternative of powering maritime applications?"

The question will be answered by:

- Conduct an experimental work of an Open Flange SOFC test-stack fuelled by three variations of ammonia concentration, pure hydrogen, and a mixture of hydrogen and nitrogen to simulate pre-cracked ammonia over a range of temperatures.
- Develop an electrochemical model of the cell as a method of estimating certain fuel cell parameters.
-

1.5 Limiting Boundaries

Ammonia
The experiment was conducted using the lab facilities and equipment at the University of Agder, Grimstad. There were hopes of installing pure ammonia during the period of this project but due to economical and safety reasons was this not a feasible option. Instead, an aqueous solution of ammonia was used to operate the cell. At the end of the project, it was intended to do a long-term run of the cell, but due to long delivering time for the new bottle of ammonia was this not completed.

SOFC
The tested cell is an Open Flange SOFC without sealing, meaning it operates at very low fuel utilisation. This aspect is therefore not considered in this study.

2 Theory

The previous chapter ended by defining the research question of this thesis. This chapter will look at ammonia as fuel for maritime application based on cost and emission of production, distribution, and viable option of ammonia power generation. Next, the fundamentals of SOFC are elaborated with focus on utilising ammonia as fuel. At last is necessary thermodynamics and fuel cell fundamentals to develop a simple fuel cell model presented.

2.1 Ammonia as Sustainable Fuel in Maritime Applications

Ammonia has in the recent years been recognised as a carbon-free hydrogen carrier with one of the biggest potentials along with methanol of eventually replacing fossil fuels in maritime applications[4], [5], [7]. Besides being a carbon free alternative, ammonia benefits from an already existing infrastructure, superior transport- and storage properties and relatively high volumetric energy density compared to hydrogen. As seen in table 3, compressed- or liquefied hydrogen requires several hundred bars or a temperature only 20°C above absolute zero, whereas ammonia can be liquified at moderate pressures in room temperatures, reducing the complexity and therefore the overall cost of the system. The process of liquify and store hydrogen is also a very energy intensive process reducing the overall efficiency of the lifecycle.

Table 3 Comparison of energy density and storage properties of some fuel alternatives.

Fuel Type	Energy Density [MJ/kg]	Volumetric Energy Density [GJ/m³]	Storage Properties	
			Pressure [bar]	Temperature [°C]
Maritime Gas Oil	42.8	36.6	1	20
Liquid Ammonia	18.6	12.7	1 or 10	-33 or 20
Liquid Hydrogen	120.0	8.5	1	-253
Compressed Hydrogen	120.0	7.5	700	20
Methanol	19.9	15.8	1	20

Downsides of ammonia is its toxic- and strong alkaline properties demanding significant security measures and procedures to ensure human and environmental health. This is an potential issue regarding ships with passengers as well as storage and bunkering in docs with high populations due to strict safety regulations associated with handling of ammonia[14]. Another obstacle is the emission and cost associated with the hydrogen supplied in the ammonia synthesis. In 2020 more than 95% of the global hydrogen production was based of natural gas and coal[15], and a transition towards electrolysis or other methods powered by sustainable energy will be essential if shall ammonia be considered an alternative of sustainable fuel. Low electricity prices and political regulated fees of fossil fuels are needed to get the cost hydrogen-holding fuels at a compatible level. The cost of hydrogen production powered by electricity is naturally dependent of the electricity price of the region as well. The topic of production and economics of hydrogen is further elaborated in the following sub-chapters.

2.1.1 Ammonia Production

Ammonia is a very energy intensive process standing for around 1.8% of the total global energy demand and an annually emission of approximate 500 million tonnes of CO_2[7]. Methods to decarbonise the ammonia production must be developed and implemented if ammonia shall be considered a clean energy carrier for transport fuel. Thus, ammonia is divided into three categories; brown-, blue- and green, dependent on the GHG emission associated with the production. Table 4 presents the methods used to produce each category as well as estimated energy consumption and carbon dioxide emissions for best available technology (BAT) in 2020 and potentials of 2050[16]. Brown ammonia is mainly produced through the highly carbon intensive steam methane reforming (SMR), and blue ammonia is made by the same processes but has implemented methods for Carbon Capture and Storage (CCS). Green category is zero-carbon ammonia produced with hydrogen made through electrolysis powered by sustainable electricity[7]. Using excess wind power to run the electrolysis is a good example of a beneficial way store excessive wind power.

Table 4 : Energy consumption and CO2 emission for Best Available Technology (BAT) for brown, blue and green ammonia production based on high pressure ammonia synthesis loop[16]*. Potential column is referred to year 2050.*

	Energy Requirement (GJ/t_{NH3})		**CO_2 Footprint (t_{CO2}/t_{NH3})**	
	BAT	**POTENTIAL**	**BAT**	**POTENTIAL**
Brown Ammonia	**26**	**26**	**1.6**	**1.6**
SMR	26	26	1.6	1.6
Heavy Fuel Oil	38	-	3.0	-
Coal	42	-	3.6	-
Blue Ammonia	**33**	**26**	**0.4**	**0.2**
SMR with CCS	33	27	0.4	0.2
Coal with CCS	57	-	1.1-2.0	0.5
e-SMR	-	26	-	1.1
Green Ammonia	**33**	**26**	**0.1**	**0.0**
Low temperature electrolysis	33	31	0.1	0.0
High temperature electrolysis	-	26	-	0.0
Biomass	-	33	1.1-1.2	0.5
Global Average	**35**	**27**	**2.0**	**1.4**

2.1.2 Clean Hydrogen

More than 95% of the global hydrogen production in 2020 was produced through methods associated with natural gas and coal, meanwhile only 0.1% was produced through electrolysis and just above 3% as by-products from chlorine production[15]. Significant decarbonation of the hydrogen production must be in place if ammonia shall be considered a clean energy carrier for transport fuel. Two proposed methods to produce low-carbon or clean hydrogen is electrolysis and implementation of CCS. The demand and production volume of clean hydrogen from electrolysis is expected to gradually increase over coming years, while CCS is simultaneously under development.

Electrolysis is used to extracting hydrogen from water is in principle a fuel cell in reverse. It is expected a significant growth of electrolysis project in the coming decade, and more is planned every year. As seen in Fig 5, the projections in 2020 of low-carbon- and clean hydrogen production volume was 6.7 million tonnes by 2030, while the year before was just planned to be 2.3 million[14], witnessing about an increasing rate of interest in electrolysis projects. It is expected that the cost of clean hydrogen will reduce faster than earlier anticipated due to reducing CAPEX, levelized cost of energy (LCOE) and a continuous improvement of utilisation levels. CAPEX is expected to decline due to the expected growth within the marked, increasing the electrolysis supply chain. LCOE is caused by beneficial pricing of clean energy, especially solar. At last, the utilisation level increases due to the increase of renewable energy project, meaning there is more clean power to power electrolysis[14]. Predicted cost of producing 1kg hydrogen the next decade is found in Fig 6, showing that cost of grey and blue hydrogen may break even by 2050.

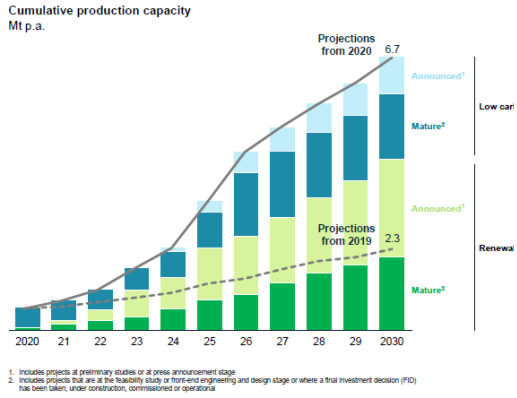

Figure 5 Planned and predicted electrolysis project the coming decades [14].

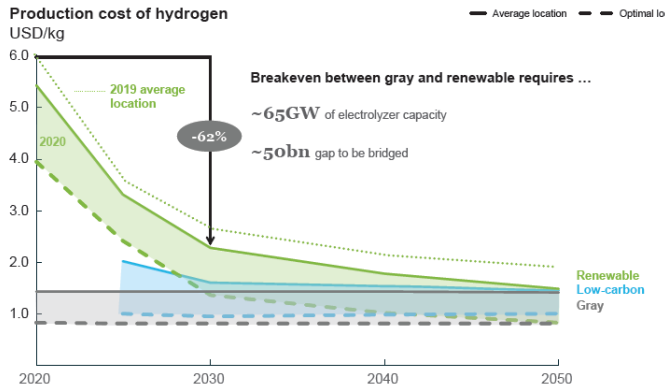

Figure 6 predicted green, blue, and grey hydrogen prices to 2050[14]

Development of CCS is a solution of reducing the overall emissions by transporting GHG emissions from fossil fuels back into the ground for storage and is based on the expectation of fossil fuels to have a significant share of the global energy consumption for several years to come. The basic principles of this technology were first used around 1970 to increase the oil production at an American oil rig, and today is more than 23 million tonnes of CO_2 stored under the Norwegian oil field Sleipner[17]. The extraction of CO_2 from a mixture of chemicals requires

a lot of heat and most efficient in combination with systems providing usable waste heat. Producing hydrogen by SMR is a system delivering sufficient waste heat and reduced the emissions by 71-92%[18] or completely[17] in combination with CCS. Nevertheless, CCS is still an immature technology and faces technical, economical, and commercial challenges. High cost, uncertain consequences associated in case of leakage, and uncertain measuring of the stored gas are some of the topics that need more research[19].

2.1.4 Green Ammonia Production

Haber Bosch is currently dominating the commercial production of ammonia. Three parts H_2 is reacted with one-part N_2 to form ammonia (NH_3). The synthesis is under high pressure (>100 bar) and temperatures (~500°C) over a Fe-based catalyst[7]. The synthesis reaction of presented in Eq. (2.1.1)

$$N_2 + 3H_2 \leftrightarrow 2NH_3 \qquad \Delta H_f^0 = -90.8\,{}^{kJ}/_{mol} \qquad \text{Eq. (2.1.1)}$$

The ammonia production plants rely heavily on steam reforming of natural gases to produce the hydrogen required. Coal, heavy fuel oil and naphtha are other alternatives, but not commonly used due to an increased CO_2 emission (2.5-3.8 CO_2/NH_3 compared to 1.6 CO_2/NH_3 for natural gas)[7]. A more comprehensive overview is found in table 5 back in the previous chapters.
A flow diagram of the production of green ammonia is presented in Fig 7. As previously mentioned, SMR to produce hydrogen is the biggest contributor of GHG emission in the ammonia production. A significant reduction can be made if hydrogen is made through electrolysis powered by sustainable energy sources, such as wind or solar powerplants.

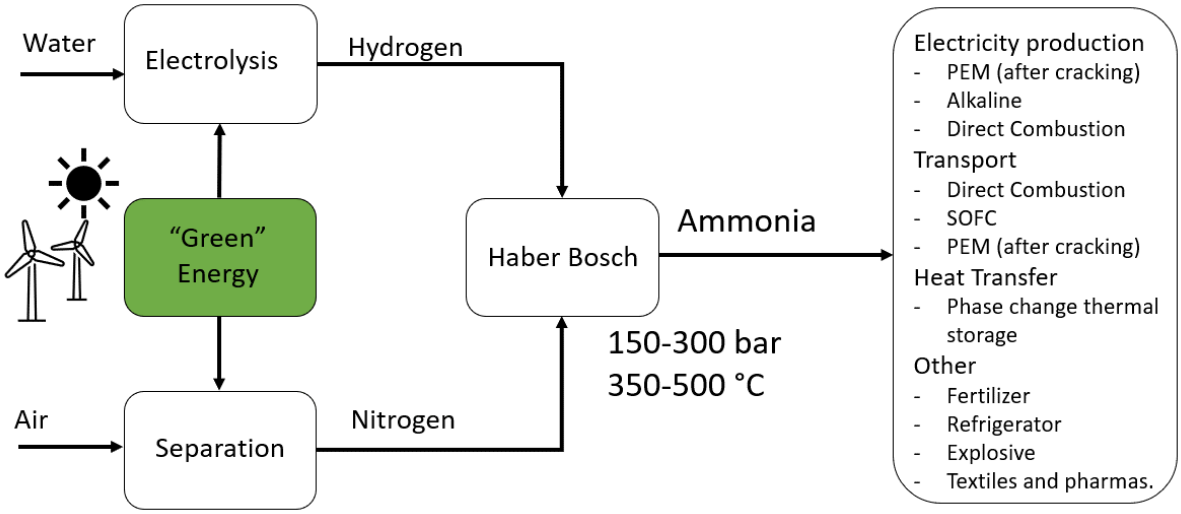

Figure 7 Example of clean production of Ammonia

2.1.1 Ammonia Power Generation in the Maritime Applications

There exist numerous methods of utilising ammonia as a power generation fuel ranging from steam- and gas turbines, various types of fuel cells and internal combustion engines (ICE). Of the mentioned alternatives Niels de Vries concluded in his M.Sc. thesis [20] that only two options are feasible for offshore power generation; ICE and SOFC. SOFC delivers the highest efficiency of the two, but high costs, slow response to load changes, and low power density results in ICE being considered an overall better option at the current state of development. This conclusion is substantiated by reports published by big institutions and companies[2], [5], [14]. DNV GL predicts in their maritime forecast report that ICE fuelled by ammonia can hold 40% of the total share of fuel consumption in the maritime industry by 2050 for scenarios with low-electricity price. The development of energy share in the maritime sector for the given scenario can be seen in the leftmost picture in Fig 8, with the final share in 2050 to the right.

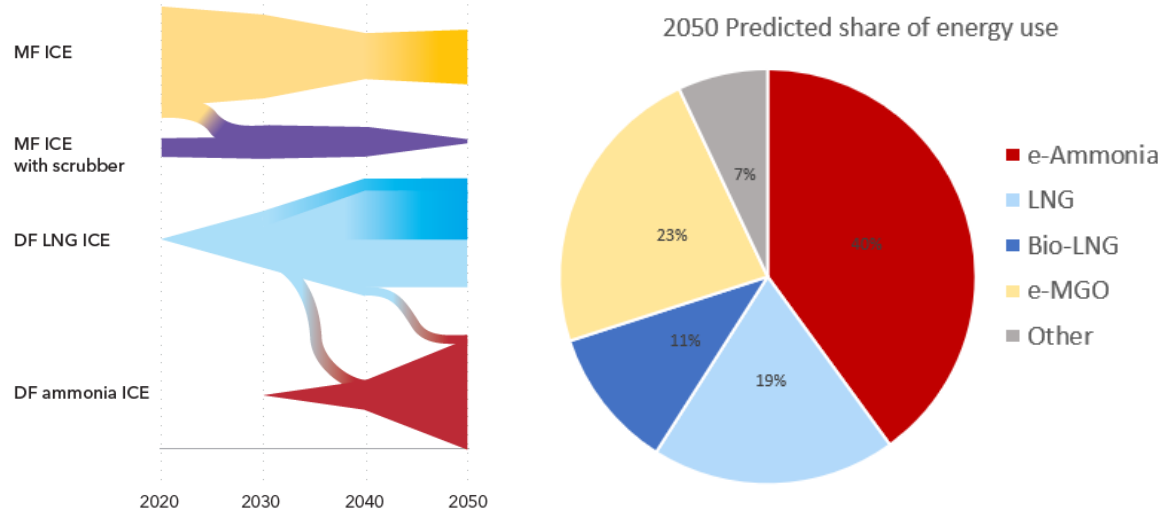

Figure 8: Predicted share of energy use in the maritime sector for low-electricity price scenarios[5].
LNG: Liquid Natural Gas, e: indicates fuel based on clean hydrogen, MGO: Marine Gasoil

2.3 Solid Oxide Fuel Cells

SOFC is a high-temperature fuel cell commonly operated between 600-1000°C and is regarded a leader among clean power generation systems in terms of conversion efficiency, fuel flexibility and environmental impact[9]. High operating temperature means high reactions rates can be achieved without the presence of precious and rare catalyst needed by low-temperature (LT) fuel cells, while also enabling reforming and cracking directly in the cell. This means hydrocarbons and ammonia can be used without pre-processing, removing the need of external reforming- and cracking units, and thereby reduce the need of free area and overall cost. The heated off-gas can be used as high-quality waste-heat to provide energy to external systems such as endothermic reformers, fire gas turbines or in combined heat and power (CHP) systems to increase the overall efficiency of the SOFC system. An example of the latter is presented by Eshan Baniasadi et al. [21] who achieved an exergy efficiency of ~85% in their CHP system containing a SOFC with heat recovery option.

Unfortunately, SOFC is victim for an unacceptable rate of degradation, high cost of materials, and long start- and stop cycling[22]. Many of these issues are related to high operating temperature, so reducing the operating temperature while maintaining the performance is therefore one of the most researched aspects of SOFC. Challenges associated with this topic is further elaborated in chapter 2.3.3

2.3.1 SOFC Build-up

SOFC is usually composed by a solid oxide-ion conducting electrolyte between porous anode and cathode electrodes. The layers can be clearly seen in Fig 9, showing a micrograph of a anode-supported single cell taken from a study by Guangyao Meng et al.[23] along with a simple home-made schematic presentation.

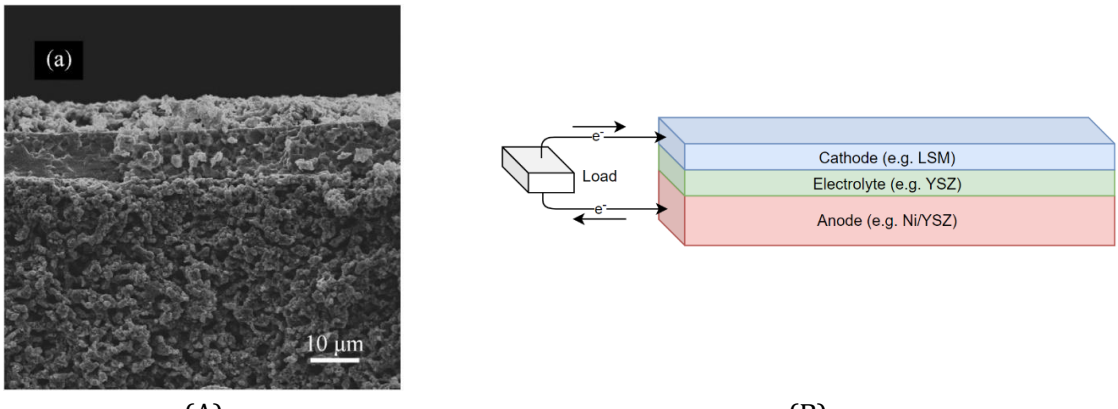

(A) (B)

Figure 9 Cross section of a nickel-based anode supported SDC electrolyte SOFC (A) and a simple schematic (B)

The electrolyte acts as a wall separating the anode and cathode chambers with the purpose of preventing gas molecules from flowing through, while simultaneously conduct reduced oxygen ions from the cathode to the reaction occurring in the anode. A good electrolyte prevents leakage flow between the anode and cathode, have high ion-conducting abilities, and has mechano-thermal properties that matches the ones of the electrodes[24]. The current state-of-the-art electrolyte is yttria (Y_2O_3) stabilised zirconia (ZrO_2), known as YSZ, and is based on a discovery from the late nineteenth century, by the German scientist Walther Nernst. He developed a ceramic electrolyte consisting of 85 mol% ZrO_2 and 15 mol% Y_2O_3. ZrO_2, also known as

Zirconium Dioxide, and is the key material in modern solid electrolytes with high oxide-ion conductivity at higher temperatures[9]. A challenge of YSZ has been low conductivity at LT and intermediate temperatures (IT) resulting in significant ohmic losses and thereby reduced performance of the cell. A hot topic within the subject of SOFC is therefore to develop new materials that performs well at lower temperatures. This is further discussed is chapter 2.3.3.

The main responsibility of the anode is to oxidate hydrogen and transfer released electrons away from the surface between the electrode and electrolyte, often known as the triple-boundary layer (TBL), and to a connected load. Porous materials are used to give supplied reactants easy access to the TBL as well as contributing to fast removal of products to release space for the reactions. In cases where ammonia or hydrocarbons are used is high catalytic activity of the cracking and reforming processes also required. The anodes today are mostly made of porous nickel-based cement mixed with other materials such as YSZ or SDC[12]. Especially Ni/YSZ has been used due to its stability, high electronic and ionic conductivity, as well as high catalytic activity for hydrogen oxidation[25].

The cathode transport electrons arriving from the connected circuits into the TBL to reduce oxygen into oxide ions. Similarly, the anode, it consists of a porous material for easy access and removal of gas and is catalytic favourable for oxygen reduction. High-temperature cathodes are often made of Strontium-doped lanthanum manganite ($La_{0.8}Sr_{0.2}MnO_{3-\delta}$, LSM), while strontium-doped lanthanum ferro-cobaltite (LSFC) and strontium-doped barium ferro-cobaltite (BSFC) is investigated option at lower temperatures[26]. YSZ and lanthanum does however react with each other, forming an insulating layer of $La_2Zr_2O_7$ preventing the flow of ions. This would result in a significantly reduced performance but is solved by including an interlayer made of ceria-based between the cathode and electrolyte[27].

2.3.1 Working principles – Hydrogen

Pure hydrogen is considered the most basic and conventional method of fuelling fuel cells due to having few to zero side reactions and requires little pre-preparation before use. The chemical reactions of a hydrogen fuelled SOFC presented by Eq. (2.3.1) to Eq (2.3.3) and a visualised by Fig 10. Oxygen or air is supplied to the cathode where it is reduced to negative charged oxygen ion (O^{2-}). The cathode is positive charged (+) so the oxygen ions is therefore conducted through the electrolyte to the negative charged (-) anode. Hydrogen in the anode is oxidised to hydrogen ions which reacts with the negative oxygen ion to form water.

$$Overall\ reaction: \quad H_2(g) + \frac{1}{2}O_2(g) \leftrightarrow H_2O(g) \qquad \text{Eq. (2.31)}$$

$$Anode: \quad H_2 + O^{2-} \leftrightarrow H_2O + 2e^- \qquad \text{Eq. (2.3.2)}$$

$$Cathode: \quad \frac{1}{2}O_2 + 2e^- \leftrightarrow O^{2-} \qquad \text{Eq. (2.3.3)}$$

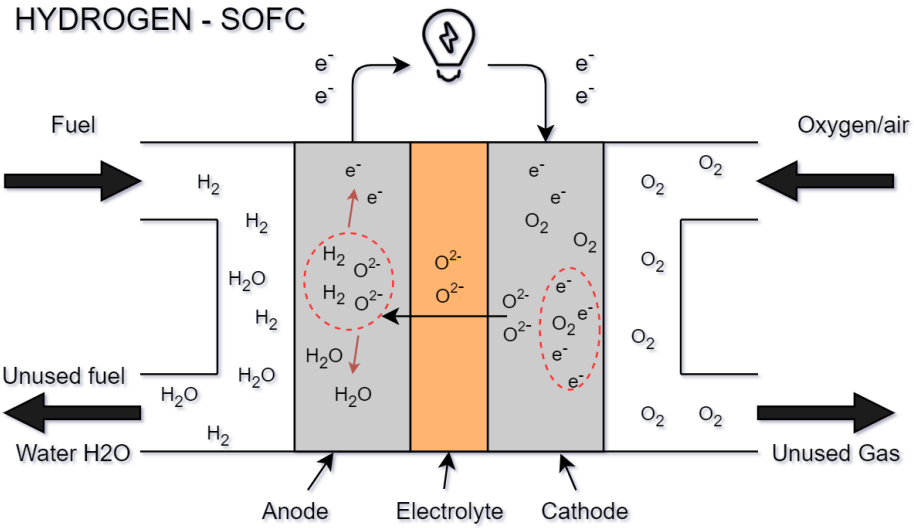

Figure 10 Sketch of SOFC fuelled by hydrogen and oxygen.

2.3.2 Working principles – Ammonia

One of the biggest advantages of SOFC is the fuel flexibility, allowing hydrogen-holding fuel to be internally reformed or cracked. Cracking ammonia directly in SOFC is a novel method of power generation that has proved to perform almost equally good as pure hydrogen[11], [28]. The reaction in Eq. (2.3.4) displays the endothermic reaction of cracking ammonia, while Eq. (2.3.5) to Eq. (2.3.7) presents overall-, anode-, and cathode reaction of the cell. Cracking of ammonia requires a fitting catalyst to be done effectively and nickel, which is the common choice of material in SOFC anode, has proved to be a great catalyst material. A schematic of ammonia supplied SOFC is displayed in Fig 11.

$$2NH_3(g) \leftrightarrow 2N_2(g) + 3H_2(g) \qquad \Delta H_f^\circ = 90.8\,{}^{kJ}/_{mol} \qquad \text{Eq. (2.3.4)}$$

$$Overall\ reaction: \quad 4NH_3(g) + 3O_2(g) \leftrightarrow 2N_2(g) + H_2O(g) \qquad \text{Eq. (2.3.5)}$$

$$Anode: \quad 2NH_3 + 3O^{2-} \leftrightarrow N_2 + 3H_2O + 6e^- \qquad \text{Eq. (2.3.6)}$$

$$Cathode: \quad O_2 + 2e^- \leftrightarrow 2O^{2-} \qquad \text{Eq. (2.3.7)}$$

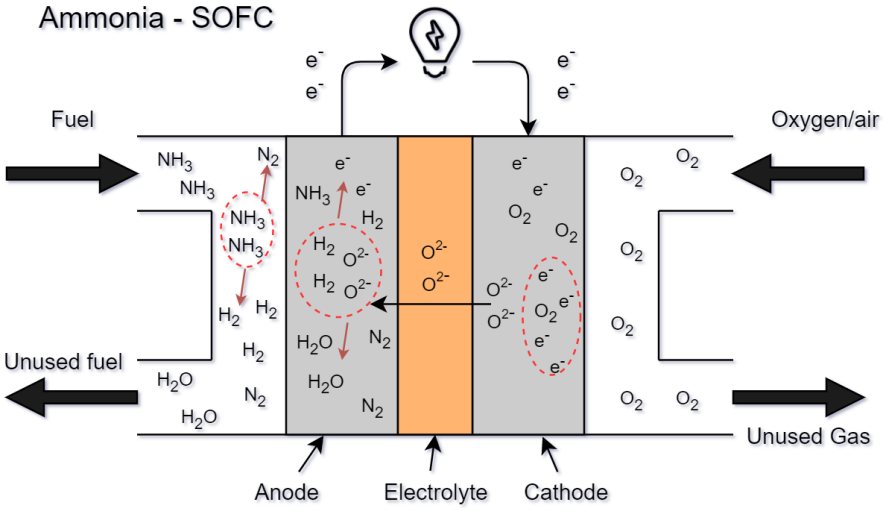

Figure 11: Sketch of SOFC fuelled by ammonia and oxygen - made in app.diagram.net drawing software.

Hydrogen and oxygen are the essential substances required to operate the cell, while nitrogen is only included due to its presence in air and ammonia. This can be seen in the overall reaction of the cell, showing the same amount of nitrogen (N_2) on both sides. However, a possibility that is being investigated is the formation a less favourable partial oxidation reaction to form nitric oxide (NO), seen in Eq. (2.3.8). NO is formed when oxygen and nitrogen is reacted under high pressures or temperatures[29], such as those found in SOFC. Studies have found the amount of NO to be almost negligible oxide-conducting SOFC fed by ammonia fed[11], [30] .

$$formation\ on\ NO: \quad 4NH_3 + 5O_2 = 4NO + 6H_2O \qquad \text{Eq. (2.3.8)}$$

2.3.3 Electrolyte Challenges and Development

The United Stated Department of Energy has since 1995 worked in a program focused on research and development of SOFC technologies. Their five goals of development is to[31]:

- Improve efficiency of SOFCs to 60 percent without incorporating carbon capture and sequestration.
- Achieve a proven lifetime of 40,000 hours or more.
- Achieve less than 0.2 percent per 1,000 hours of degradation rate.
- Decrease the stack costs of SOFCs to less than $225 / kilowatt (kW).
- Decrease system SOFC costs to less than $900 / kW.

Downsides of operating at high temperatures (800-1000°C) are regarded more significant than the benefits. High cost of feasible materials and mandatory sub-systems, reduced durability, as well as long start- and stop cycles of the cell[22] are some of the issues followed by high operating temperatures. Degradation issues remains of the biggest challenges and per 2019 was there no documented reports of a SOFC operating at $\geq$40 000 with less than the 0.2% degradation rate[31]. One of the most researched aspects of SOFC is therefore methods to lower the temperature while maintaining performance[24], but there are still obstacles that needs solving. A challenge has been the highly temperature-sensitive conductivity of the YSZ electrolyte, resulting in reduced conductivity and thereby a significant loss when operating at IT and LT. The ohmic losses η_{el} in the electrolyte is proportional to the area specific resistance (ASR) of the electrolyte and the current density *j.* The term of ohmic loss and ARS is expressed by Eq. (2.3.9) and (2.3.10):

$$\eta_{el} = ASR * j \qquad (2.3.9)$$

$$ASR = \frac{\tau_{el}}{\sigma_{el}[T]} \qquad (2.3.10)$$

Where τ_{el} is the thickness of the electrolyte layer and σ_{el} is the conductivity at temperature T. The expression above shows that ASR, and thereby the losses, of the electrolyte can be kept at an acceptable level LT and IT by two means: reducing the thickness of the electrolyte layer or develop materials with higher conductivity[24]. Decreasing the electrolyte layer of YSZ-based cell from ~150µm to ~10µm, and use electrodes to support the mechanical durability is an established method of reaching IT with acceptable electrolyte performance[22]. Producing thin electrolytes with acceptable performance at LT requires advanced processes that is still need

development[24]. The other measure mentioned is to develop new variants of electrolytes. YSZ is the state-of-the-art material and benefits from high physico-chemical stability but the conductivity is significantly reduced at IT and LT in comparison with many of the competitive alternatives, seen clearly in Fig 11. Cerium Gadolinium Oxide (CGO), Gadolinia doped Ceria (GDC), Scandia-stabilised zirconia (ScSZ), and perovskite-based electrolyte are some options showing both beneficial and disadvantageous properties. The first two mentioned (CGO and CDC) has proved to have high conductivity at lower temperatures compared to YSZ but contain costly and rare materials that is mechanical unstable and struggles during operation with low oxygen partial pressure. ScSZ has improved conductivity and stability compared to YSZ with the same operational conditions but is also suffering from being a rare and expansive material[24].

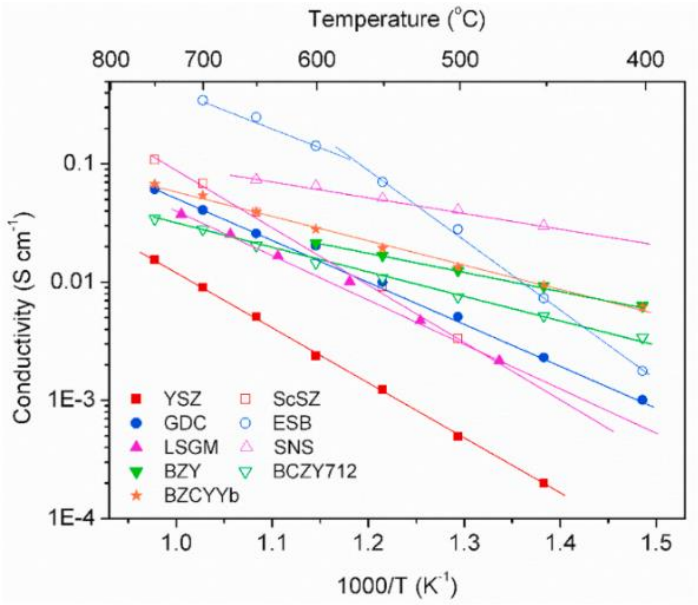

Figure 12: Comparison of the conductivity of various electrolyte materials[24]

2.3.4 Ammonia in SOFC

Several studies the last few decades have showed promising results of ammonia as a feasible fuel in SOFC systems. As early as 2003, Hugh Middleton et al. [11] demonstrated the feasibility of ammonia in a tubular SOFC when they obtained results almost identical to the ones of hydrogen while operating over a silver anode with an iron-based catalyst and with a platinum anode at temperature between 700 and 1000°C. The latter even reach efficiencies applicable to commercial applications, but platinum is not a regarded practical solution due to its high cost. The anode commonly used today consists of nickel which has proven to be a very good catalyst for ammonia cracking. G. Cinti et al. [13] presented a study of 4 anode supported planar single cells stack consisting of Ni/8YSZ anode, 8YSZ electrolyte and LSM/8YSZ cathode resulted in a maximum voltage reduction of 2% compared to results obtained by hydrogen in the range of 700-800°C.

A collection of power- and current densities at a typical operating voltage of 0.7V of relevant studies is presented in table 5.

Table 5 Collection of relevant papers

SOFC Type	Temp. [°C]	Anode/ Cathode/ Electrolyte	Catalyst	Fuel	OCV Voltage [V]	Power Density [mW/cm2]	Current density [mA/cm²]	Ref
Tubular	700	A: Ni/YSZ C: LSM E: YSZ	Nickel	NH_3	1.04	35	50	[28]
				$0.4NH_3$/ $0.6H_2$	1.10	38.5	55	
				H_2	1.12	42	60	
	650	A: NiO/SDC C: BSFC E: SDC	Ni-SDC	H_2	0.747	875	1250	[23]
				NH_3	0.768	560	800	
	900	A: Ag C: YSZ E: YSZ	Fe	0.1 H_2	-	0.385	0.55	[11]
				NH_3	-	0.210	0.6	
			Non	NH_3	-	0.056	0.08	
		A: Pt	Pt	NH_3	-	70	100	
	750	A: BZCY + NiO C: BSCF E: BZCY	Nickel	H_2	~1	350	550	[32]
				NH_3	0.98	310	500	
Planar	750	A: Ni/YSZ C: YSZ E: LSCF	Ba-Ni/YSZ	NH_3	1.09	262.5	375	[12]
				H_2	1.09	266	380	
	650			NH_3	1.15	98	140	
				H_2	1.15	105	150	
	500	A: Ni-SDC C: SSC-SDC E: SDC	Ni-based	NH_3	0.9	35	50	[10]
				H_2	0.95	52.5	75	
	700			NH_3	0.87	105	150	
				H_2	0.87	105	150	
	650	A: Ni-CGO C: BSCFO-CGO E: BCGO	Nickel	H_2	1.15	210	300	[33]
				NH_3	1.1	175	250	

2.4 Fuel Cell Modelling

This chapters are meant to give the theoretical foundation of thermodynamic- and fuel cell theory used to develop electrochemical fuel cell models. Expressing fuel cell behaviour by mathematics can be done by taking advantage of thermodynamic and fuel cell equation and theory. The thermodynamic quantities of enthalpy and entropy are used to derive the released energy of the reaction and the theoretical OCV of the cell. As the current increases, the cell is exposed to various polarisation losses, namely activation-, ohmic- and diffusion losses. These can be explained by various approaches but the ones used in this report is based a selection of papers [34], [35], [36], [37],[8]. Assumption made are that the temperature and pressure are held constant, and the gas behave as ideal gas.

2.4.1 Thermodynamics

Understanding the thermodynamic properties of the chemical reaction in the fuel cell is the first step of understanding fuel cell behaviour. Enthalpy and Entropy, presented as H and S respectively, are fundamental terms in fuel cell thermodynamics and is used along with temperature to calculate GFE, denoted as G. Enthalpy describes the internal energy of a reaction, and entropy can be explained as the quality of energy. GFE is a sum of these and describes the energy that can actually be used to do external work, which in case of fuel cells are the capability of pushing electrons through an external circuit[8]. GFE is further elaborated in the next subchapter, meanwhile this chapter will go through the steps of deriving the enthalpy and entropy as a function of temperature using tabulated values and heat capacity factor C_p.

Standard enthalpy- and entropy of formation of relevant substances are obtained from tables found in textbooks about thermodynamics [38][39][40] and are reproduced in table 6. The term '*standard*' refer to conditions corresponding to 298.15K (25°C) and 1 bar (0.1MPa). Calculating the standard enthalpy and entropy of the fuel cell reaction is done by applying Hess's law, presented in Eq. (2.4.1) and Eq. (2.4.2).

Table 6: Standard thermodynamic quantities of relevant substances, adopted from [38].

Substance		State	ΔH_f^0 Enthalpy [kJ/mol]	ΔS_f^0 Entropy [J/mol K]	ΔG_f^0 GFE [kJ/mol]
Hydrogen	H_2	g	0,0	130,7	0,0
Ammonia	NH_3	g	-45,9	192,8	-16,4
Water (Steam)	H_2O	g	-241,8	188,8	-228,6
Nitrogen	N_2	g	0,0	191,6	0,0
Oxygen	O_2	g	0,0	205,0	0,0

$$\Delta H^o_{f_{reaction}} = \sum \Delta H^o_{f\ Products} - \sum \Delta H^o_{f\ Reactants} \quad \text{Eq. (2.4.1)}$$

$$\Delta S^o_{f_{Reaction}} = \sum S^o_{f\ Products} - \sum S^o_{f\ Reactants} \quad \text{Eq. (2.4.2)}$$

Reactants are the supplied substance and is usually located on the left side of the equation, while products can be defined as the end state. Because the fuel cell is operating at temperatures around 750°C (significantly higher than 25°C) necessary corrections must be made by integrating the heat capacity factor C_p as shown in Eq. (2.4.3) and Eq. (2.4.4):

$$\Delta H_T^0 = \Delta H_{298K}^0 + \int_{298K}^{T_2} \Delta C_p \, dT \qquad \text{Eq. (2.4.3)}$$

$$\Delta S_T^0 = \Delta S_{298K}^0 + \int_{298K}^{T_2} \frac{\Delta C_p}{T} \, dT \qquad \text{Eq. (2.4.4)}$$

Where ΔH_T^0 and ΔS_T^0 is the change of enthalpy and entropy of the reaction at temperature T_2, ΔH_{298K}^0 and ΔS_{298K}^0 is the standard values at temperature 298K, and ΔC_p is the heat capacity factor (HCF) of the reaction. The most accurate result is achieved by obtaining tabulated HCF of chemicals from textbooks but are often limited by temperature range and available chemicals. Ammonia is a good example of a substance that may be difficult to find in tables, especially at temperatures relevant for SOFC. Fortunately, textbooks containing equations and coefficients derived from empirical results are available for a wide range of substances and temperatures. HCF of relevant substances is calculated using Eq. (2.4.5) in combination with tabulated heat capacity coefficient (HCC) found in table 7[39].

$$\Delta C_{p0} = C_0 + C_1\theta + C_2\theta^2 + C_3\theta^3 \quad \theta = T(K)/1000 \qquad \text{Eq. (2.4.5)}$$

Table 7: Constant-Pressure heat capacity coefficients in units of [kJ/mol K], adopted from [39].

Substance	[kJ/mol K]			
	C_0	C_1	C_2	C_3
Hydrogen	0.027	0.009	-0.014	0.008
Ammonia	0.027	0.024	0.017	-0.012
Water (Steam)	0.032	0.002	0.011	-0.004
Nitrogen	0.031	-0.013	0.027	-0,013
Oxygen	0.028	0.000	0.017	-0.011

The HCF for the reaction can be calculated directly using Eq. (2.4.6) and Eq. (2.4.7). Where n is the number of moles of product i and reactant j, x is the HCC rank ranging from 0 to 3, and ΔC_x is the combined HCC of the reaction.

$$\Delta C_x = \sum_{Products} n_i C_x - \sum_{Reactants} n_j C_x \qquad \text{Eq. (2.4.6)}$$

$$\Delta C_p = \Delta C_0 + \Delta C_1\theta + \Delta C_2\theta^2 + \Delta C_3\theta^3 \qquad \text{Eq. (2.4.7)}$$

The final expressions to calculate enthalpy and entropy correlated for temperature is obtained by inserting Eq. (2.4.7) into Eq. (2.4.3) and Eq. (2.4.4) and integrate with respect to variable T:

$$\Delta H_T = \Delta H_{298K}^0 + \Delta C_0(T - 298) + \frac{\Delta C_1}{2 * 10^3}(T^2 - 298^2) + \frac{\Delta C_2}{3 * 10^6}(T^3 - 298^3) + \frac{\Delta C_3}{4 * 10^9}(T^4 - 298^4) \qquad \text{Eq. (2.4.8)}$$

$$\Delta S_T = \Delta S_{298K}^0 + \Delta C_0 \ln\left(\frac{T}{298}\right) + \frac{\Delta C_1}{10^3}(T - 298) + \frac{\Delta C_2}{2 * 10^6}(T^2 - 298^2) + \frac{\Delta C_3}{3 * 10^9}(T^3 - 298^3) \qquad \text{Eq. (2.4.9)}$$

The previous sections went through the steps of deriving the expression to calculate enthalpy and entropy of the reaction occurring in the cell. Most of the work of finding the GFE is already done all that remains is to sum the enthalpy and entropy quantities as shown in Eq. (2.4.10).

$$\Delta G = \Delta H_T - T\Delta S_T \qquad \text{Eq. (2.4.10)}$$

The reversible open circuit voltage E_0 is directly connected to the available energy released by the reaction and is calculated using Eq. (2.4.11). This is also known as electromotive force (EMF) and is the theoretical OCV if the cell has no losses.

$$E_0 = \frac{-\Delta G}{zF} \qquad \text{Eq. (2.4.11)}$$

Where z in number of mobile electrons per reaction (Ref chapter 2.3.1 and 2.3.2) and F is Faraday's constant. Up to this point the calculation is only adjusted for temperature, but the activity of the species involved can have a significant impact on the cell. Nernst's Equation, presented in Eq. (2.4.12), includes the activity of the involved substances as a variable in[8].

$$E = E_o + \frac{RT}{zF} \ln\left(\frac{a_J^j * a_K^k}{a_L^l * a_M^m}\right) \qquad \text{Eq. (2.4.12)}$$

Where E is the EMF of the fuel cell adjusted for both temperature and pressure, R is the universal gas constant, and a_X^x is the activity of x moles of species X. To simplify is it often assumed ideal gas behaviour, and this gives the opportunity of express the activity:

$$a = \frac{P}{P^0} \qquad \text{Eq. (2.4.13)}$$

Having P as the partial pressure of the substance and P^0 as the standards pressure, usually 1 bar. The activity of a dissolved substances dependents on the strength of the solution[8]. Steam is dependent on the vapour pressure of steam $P^0_{H_2O}$, found in tables.

$$a = \frac{P_{H_2O}}{P^0_{H_2O}} \qquad \text{Eq. (2.4.14)}$$

2.4.2 Fuel Cell Polarization

In the previous chapter the theoretical potential of the cell was eventually derived using Nernst's equation and thermodynamic quantities. However, in actual fuel cells the potential is lower than the theoretical value due to various polarisation losses. As seen in Eq. (2.4.15), the actual output voltage V_{fc} affected by three main losses: *activation loss, ohmic loss and concentration loss.* These can be identified at the polarisation curves as seen in Fig. 14.

$$V_{fc} = E - \eta_{act} - \eta_{ohm} - \eta_{con} \qquad \text{Eq. (2.4.15)}$$

E is Nernst reversible voltage, η_{act} is the activation loss, η_{con} is the concentration loss, and η_{ohm} is the ohmic loss. Each part of the equation is further elaborated in the following subchapters.

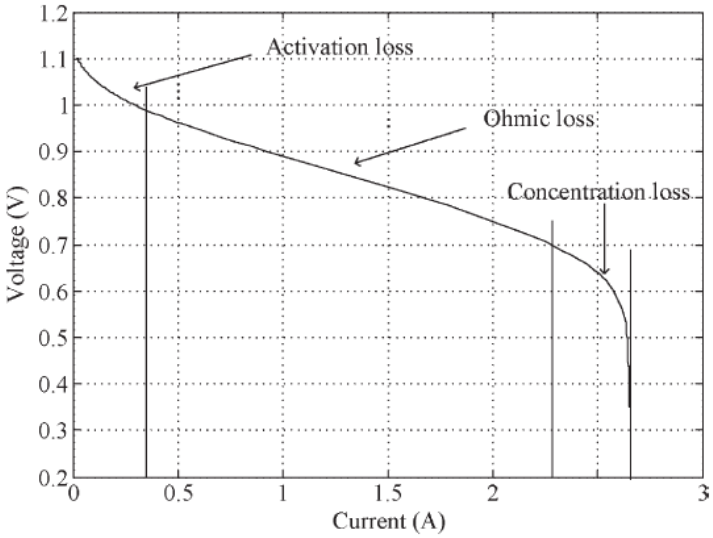

Figure 13 Typical polarisation curve for fuel cells[8]

2.4.3 Activation Polarisation

Activation polarisation represent the energy needed to keep the reaction occurring. This is visualised in Fig 14 as the height of the curve the reactants J and K must overcome to become product L and M. Catalysts, such as nickel in SOFC, are used to reduce the need of energy and thereby increase the rate of the reaction[41]. Earlier was activation polarisation in SOFC often neglected due its high operating temperature, but as the temperature has been reduced to below 1000°C it has become an important factor to take into consideration[42].

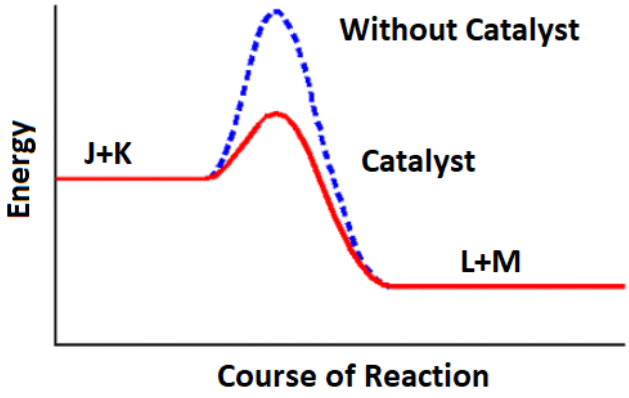

Figure 14 Activation Energy[41]

The general expression of activation energy is expressed by the Butler Volmer equation presented in Eq. (2.4.16)[42].

$$I_{fc} = I_0(e^{(\frac{\alpha_1 nF}{RT})\eta_{act}} - e^{(-\frac{\alpha_2 nF}{RT})\eta_{act}}) \quad \text{Eq. (2.4.16)}$$

Where I_{fc} is the fuel cell current, i_0 is the current exchange current and α_1 and α_2 is the transfer coefficient of the oxidation and reduction process. Setting $\alpha_1=\alpha_2=0.5$ and solve for the activation polarisation simplifies the Butler Volmer equation into Eq. (2.4.17), also called the *hyperbolic sine approximation*[42]:

$$\eta_{act} = \frac{RT}{F} * \sinh^{-1}(\frac{i}{2i_0}) \quad \text{Eq. (2.4.17)}$$

The exchange currents at the anode i_{0an} and cathode i_{0ca} can be calculated using Eq. (2.4.18) and Eq. (2.4.19):

$$i_{0_{ca}} = k_{0_{ca}} * a_{O_2}^{\Upsilon} e^{(-\frac{E_{a_{ca}}}{RT})} \quad \text{Eq. (2.4.18)}$$

$$i_{0_{an}} = k_{0_{an}} * a_{H_2}^{\delta} * a_{H_2O}^{\varepsilon} * \ e^{(-\frac{E_{a_{an}}}{RT})} \quad \text{Eq. (2.4.19)}$$

Where the k_0 is pre-exponential constant, Υ, δ, and ε is values dependant on the rate of reaction. These values can be found in literatures such as [42].

2.4.5 Ohmic polarisation

The resistance in the cell is dependent on the conductivity and thickness of the anode, cathode, and electrolyte layers. Ohmic voltage polarisation is caused by the resistance ion meets when flowing through the electrolyte and the resistance electrons meets in the electrodes. It can be expressed as a function of conductivity and thickness of each layer, as seen in Eq. (2.4.20). Contact resistance due to non-ideal connections in the electric system is often included, but not implemented in this report. If implemented, it is simply added to portion within the brackets.

$$\eta_{ohm} = \left(\frac{\tau_{an}}{\sigma_{an}} + \frac{\tau_{el}}{\sigma_{el}} + \frac{\tau_{ca}}{\sigma_{ca}}\right) * j \quad \text{Eq. (2.4.20)}$$

2.5.6 Concentration and mass transfer polarisation

Concentration losses are expressed by the change of partial pressure of each participating species from the surface of the electrode and into the TLB. The expression can be seen in Eq. (2.4.21)[37], and is a adjustment of Nernst's Equation.

$$\eta_{con} = \frac{RT}{2F} * \log\left(\frac{P_{H_2O,TBL} * P_{H_2}}{P_{H_2O} * P_{H_2,TBL}}\right) + \frac{RT}{4F}\log(\frac{P_{O_2}}{P_{O_2,TBL}}) \quad \text{Eq. (2.4.21)}$$

Where P_X is partial pressure of species x at the surface of the electrode, and $P_{X,\,TBL}$ is the partial pressure at the TBL. To calculate the partial pressures at the surface is Eq. (2.4.22) to Eq. (2.4.24) applied[37].

$$P_{H_2,TBL} = P_{H_2} - \frac{RT\tau_{an}}{2F * D_{eff,an}} j \qquad \text{Eq. (2.4.22)}$$

$$P_{H_2O,TBL} = P_{O_2} + \frac{RT\tau_{an}}{2F * D_{eff,an}} j \qquad \text{Eq. (2.4.23)}$$

$$P_{O_2,TBL} = P - (P - P_{O_2}) * e^{-\frac{RT\tau_{ca}}{4F * D_{eff,ca}} j} \qquad \text{Eq. (2.4.24)}$$

Where D_{eff_an} and D_{eff_ca} is the effective diffusion coefficient of the anode and cathode respectively. The process of deriving these quantities can be tidies, and the reader is referred to [43][35] and [37] in it is of interest.

2.5 Electrochemical Impedance Spectroscopy

Electrochemical Impedance Spectroscopy (EIS) is a strong tool used to identify and unfold the characteristics of complex electrochemical systems such as a SOFC. EIS analysis makes it possible to separates the impedance of each individual process with an impact on the electron transfer resistance in the cell, all from gas diffusion at the anode and cathode to the pure ohmic resistance the electrons meets through the electrolyte, electrodes and wires[44].

Polarisation losses in a SOFC are differentiated by time constant characteristics and the response when exposed to various frequencies. The signal applied to the SOFC system goes from high to low frequencies in pre-defined range and step, and for each step of frequency the response (impedance) of the system is measured and plotted in Nyquist and bode diagram, which is analysed to characterise the ion conducting properties and electrode material performance[45].

The signal applied to the SOFC system is most commonly a sinusoidal voltage potential superimposed on a DC bias[46]. Assuming a voltage $u(t) = Ucos(2\pi ft + \varphi)$ is applied to the system, the response would be a current $i(t) = Icos(2\pi ft + \vartheta)$, where U and I is the signal amplitudes, f is the frequency, t is the time, and φ and ϑ is the phase-shift of the voltage and current respectively. This works the other way around as well; a current can be applied to receive a voltage response, based on the very basics of ohms law. The impedance of the system for the entire range of frequencies tested is derived by taking advantage of the phase shift and amplitude of the measured signal. Impedance is calculated as a function of the angular velocity $\omega = 2\pi f$ and the frequency dependant phase-shift $\phi(\omega)$ between the voltage and current. If a voltage potential *u(t)* is used as excitation signal the expression of impedance becomes[44]:

$$Z(j\omega) = \frac{u(t)}{i(t)} = \frac{U}{I(\omega)} e^{j\phi(\omega)} = |Z(\omega)|e^{j\phi(\omega)} = Re\{Z(\omega)\} + jIm\{Z(\omega)\} \qquad (X)$$

Admittance $Y(\omega)$ is the inverse of impedance ($Y(\omega) = \frac{1}{Z(\omega)}$). And is used to describe the dynamic response, or transfer function, of the system. Transfer functions is useful when making dynamic models of the system[46].

It should be noted that three conditions must be fulfilled to ensure valid results from EIS analysis:

1. **Linearity** - The system response is described with help from a set of linear differential laws[46], and the applied signal can dilute the results of nonlinear system. This is a potential issue in SOFC, or other types of fuel cell systems, as multiple mass-transfers, and chemical and electrochemical processes makes them nonlinear. However, linearity can be assumed when limiting the amplitude of the applied signal to a given thermal voltage.
2. **Stability** – The system should be stable before and after the analysis.
3. **Causality** - The response of the system should not be affected by anything but the test signal.

Typical parameters used for EIS analysis of SOFC systems is 10-50mV and frequencies in the range of 0.01 Hz to 1 MHz [44][46][47].

The plotted Nyquist and bode diagram obtained from an EIS analysis displays the impedance of the system as the frequency change, and can be used as to determine the impact of parameters such as temperature, pressure, materials, and microstructure on the system[46] to mentioned some. Fig 15 presents a presentation the input and output signal, typical diagrams used to analyse the results and an example of an equivalent circuit [45].

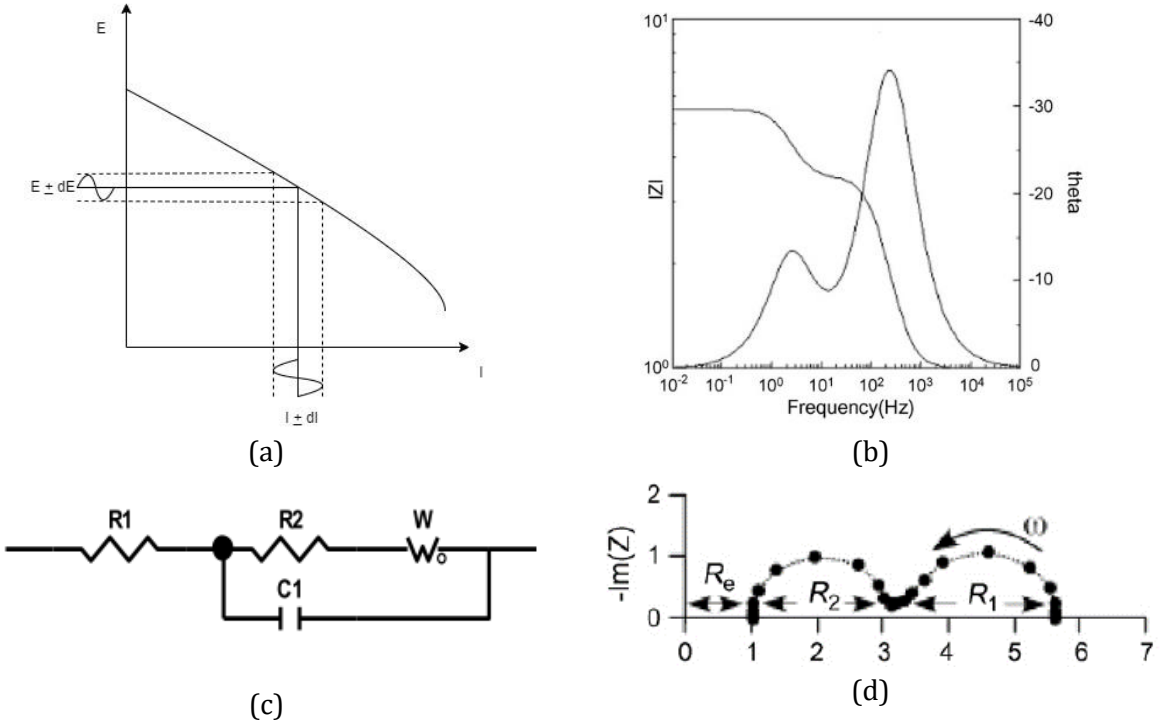

Figure 15: (a) Visualisation of I/V-curve exposed to an AC signal with a DC bias and the corresponding response from the system; (b) bode plot presenting phase-shift as a function of frequency; (c) Equivalent circuit of a SOFC fuel cell; (d) Nyquist plot of measured impedance[46][47].

EIS is a tool used identify the electrochemical performance of a SOFC, as well as the polarization characteristics of the cell. The various polarization losses have different responses to time constants and frequencies[45]. From the response a physical equivalent circuit can be developed as a tool to investigate fuel cell response without needed the actual cell. Fig 16 presents a relative advanced equivalent circuit developed by A. Leonide [44] to explain his SOFC cell, but simpler circuits will less element are also commonly used. A list of the electronic elements and its typical equivalent components in the cell is seen in table 8.

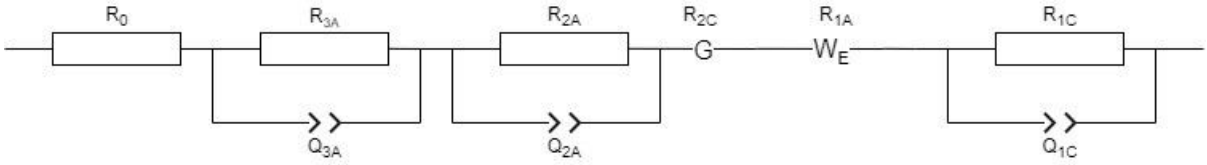

Figure 16 Equivalent circuit of a SOFC adopted from[44]

Table 8: Elements used to build equivalent circuits of electrochemical systems[45].

Elements	Explanation	Admittance 'Y'	Impedance 'Z'
R	Resistance – only real part and independent of frequency. Divided in 2: 1) Ohmic resistance 2) Polarization resistance	$\frac{1}{R}$	R
L	Inductance – Imaginary part, Current is 90° in front of voltage	$\frac{1}{jwL}$	JwL
C	Capacitance – Imaginary part. Has inverse function of frequency, and current lags 90° to voltage¨ Divided in 2: 1) Double layer capacitance (C_{dl}) 2) Coating-Capacitance (C_c)	JwC	$\frac{1}{jwC}$
CPE	Constant-Phase Element often known as 'Q' element. Used to simulate an non-ideal capacitance, which is more likely in fuel cell modelling. Often used to model C_{dl} and C_c. - Y_0 = Admittance of ideal capacitance - n = empirical constant (0-1)	$Y_0(jw)^n$	$\frac{1}{Y_0(jw)^n}$
Warburg	Used to model the diffusion of ions at the interfaces of the cell. For semi-infinite diffusion layer. - Y_0 = Diffusion admittance.	$Y_0(jw)^{0.5}$	$\frac{1}{Y_0(jw)^{0.5}}$
Gerisher	Like thin-layer diffusion element on the Nyquist-plot.	$\frac{1}{Y_0\sqrt{k+jw}}$	$Y_0\sqrt{k+jw}$

- w = 2πf (angular velocity)
- j = imaginary number
- k = rate constant parameter (complex to estimate, based of experimental derived constant)

3 Methods

A SOFC with a planar single cell has been tested with ammonia, hydrogen and a mixture of hydrogen and nitrogen as fuel. This chapter goes through the necessary details and procedures of the experimental work, all from operating properties, lab set-up and risk assessment.

3.1 Lab Experiment

3.1.1 Planar Single Cell

An Open Flange SOFC with a planar anode supported single cell composed by a Ni/8YSZ anode, 8YSZ electrolyte and a LSM cathode was tested to investigate the feasibility of using ammonia as fuel. The cell was handed out by the supervisor at the start of the project, and exact composition and geometric quantities was not following the cell. Composition was defined with help from the supervisor who handed out the cell while the thickness of the layers is estimated using a sliding canvas and typical values from literatures. Fig 17 presents the expected build-up of the single cell along with materials and geometric properties of the layers. A photo of the cell seen from above is presented in Fig 18 along with the diameter of the cell and cathode layer. The black surface area corresponds to the cathode electrode and the limiting part in regards of the active surface area. An interlayer of CGO is applied between the cathode and electrolyte for protection. This is a protective layer that prevents the cathode material, that contains strontium, from reacting with the YSZ electrolyte, that contains ZrO2. Without the CGO layer then an adverse reaction will occur that forms an insulating layer of strontium zirconate SrZrO3. The area of the cathode is later used to calculate the current density [A/m^2] which is commonly used in evaluation of fuel cell performance.

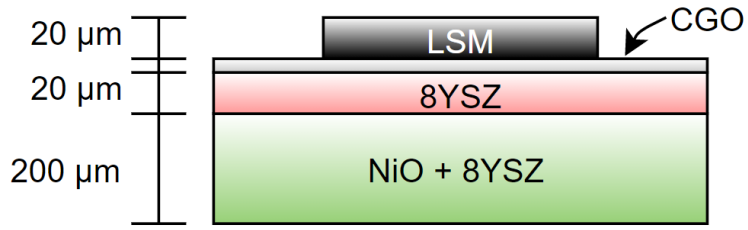

Figure 17 Sketch of the single cell with estimated thickness. (not to scale)

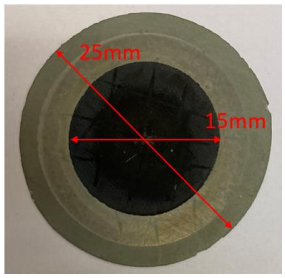

Figure 18 Single Cell from above.

3.1.2 Mass-Flow

The SOFC was operated using five variants of fuel: pure hydrogen acting as a reference (1), a 3:1 mixture of hydrogen and nitrogen to simulate pre-cracked ammonia (2), and three variants of ammonia concentration (5.9, 15.2, and 32wt%) (3-5). The cell is an unsealed open flange, resulting in a significant portion of the fuel being combusted out the sides of the cell instead of being reacted. Achieving high efficiency is not the objective of this study, but instead to investigate the performance of ammonia in comparison to hydrogen without significant impact of mass-transfer losses. This is achieved by supplying abundance amount of fuel to the reaction, even to an extent where the utilisation factor is approximate 0%. The applied flow rates are found in table 9 and was held constant during all tests.

Table 9: Flow rates of the various fuel scenarios

Fuel		Gas Supply [ml/min] Hydrogen	Nitrogen	Air
1	5.9% Ammonia	-	200	>5000
2	15,2% Ammonia	-	200	>5000
3	32% Ammonia	-	200	>5000
4	Pure Hydrogen	566	-	>5000
5	Hydrogen/Nitrogen	566	188	>5000

Hydrogen and nitrogen were provided from the gas tanks seen in Fig 19 located in an external room and air by a mini compressor. Ammonia on the other hand was supplied from a bottle of ammonia concentration washed with nitrogen to help carry ammonia vapor into the cell. The supply of ammonia is affected by the flow of nitrogen and the vapor pressure, where the latter is affected by the concentration and temperature of the solution. The only variable parameter in this study is concentration, as the temperature at 20°C and flow of nitrogen at 200 ml/min was held constant. The actual mass flow was controlled by using a manually measuring technique of flipping a filled bottle of water upside down, with the opening under water to prevent it from spilling out. When the bottle is mounted as seen in Fig 20 gas was supplied through the opening of the bottle, and the time the gas spent to replace 1L of water was taken. The time used to replace 1L gives the flowrate in min/l, and can easily be used to calculate the flow rate in terms of ml/min.

Figure 19 Tanks containing hydrogen

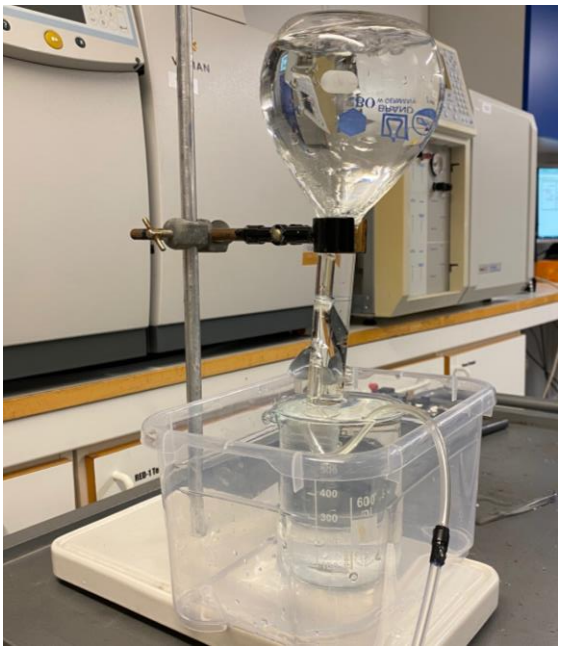

Figure 20 Measuring of the actual mass flow

The minimum moles per second required to produce a current is calculated as a function of produced current divided by the number of electrons transferred per mole of reactant and Faraday's constant. The gas usage in term of ml/min is derived by simply include the volume of ideal gas (V_{id}*=24 l/mole)* into the equation. The volumetric flow rate of gas required to produce a current between 0 and 5A is given by the plot in Fig 21. In this study however, many times the low rate of the plot in Fig 21 is supplied to avoid mass-transfer losses, even to an extent where the fuel utilisation is closer to 0% than anything else.

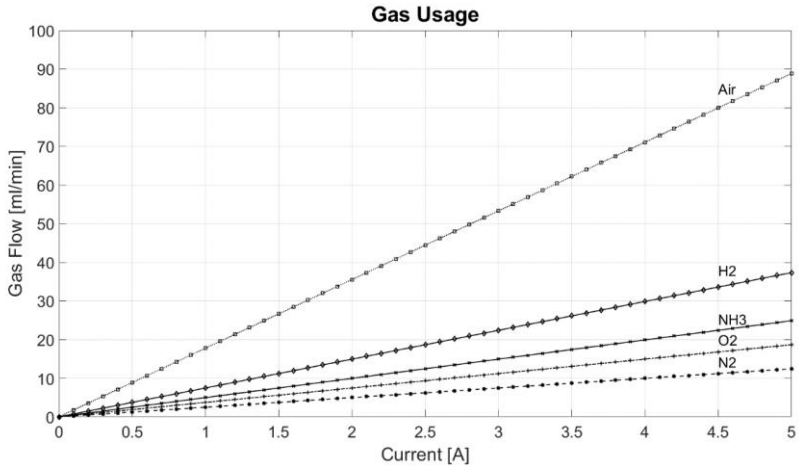

Figure 21 The amount of gas contributing to the reaction as the current increases. Higher mass flow is required as realistic fuel cell has less than 100% fuel utilisation. (Fuel utilisation < 100%).

3.1.3 Heating of Furnace

The cell was tested at temperatures ranging from 600°C to 850°C. When the furnace was heated from cold condition (20°C), it was recommended to increase the temperature slowly to the targeted temperature to avoid thermal stress and potentially damaging the components. The recommended heating program provided by the manufacturer of the test set-up is seen in Fig 22 and summarised as 6 steps:

Step

0-1: Adjustable start time
1-2: Heat 120°C/h until 400°C
2-3: Maintain 400°C at 0 hours
3-4: Heat 200°C/h until target
4-5 Maintain operating temperature
5-6 Cool 300°C/h

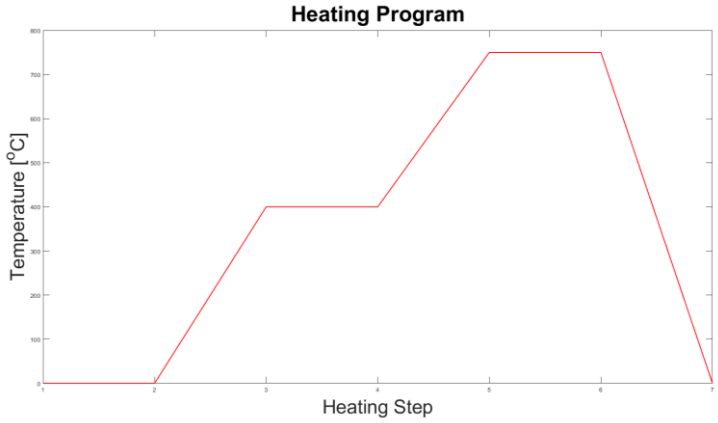

Figure 22 Visual presentation of the heating steps.

Due to the long start-up time, it was decided to reduce the initial heat time (step 2-3) by increasing heating rate from 120°C/h to 300°C/h. It was discussed with supervisor and it was concluded that the cell would likely handle the thermal stress. However, a potentially outcome was the loosening of the nickel wire welded on the anode plate used to measure the anode potential. This was discovered when the cell was dismantled after testing and caused significant delay for the next test. Waiting for repair took several days and it appeared to be more problematic than expected to weld to wire back on the plate. As seen in Fig 23, the solution became to drill a hole just able to fit the wire. This results in a somewhat unstable impedance between the wire and the cell but is not impacting the results as the wire is not conducting any currents. The cell with the nickel wire implemented is seen in Fig 24.

Figure 23 Drilling hole to reconnect the nickel wire

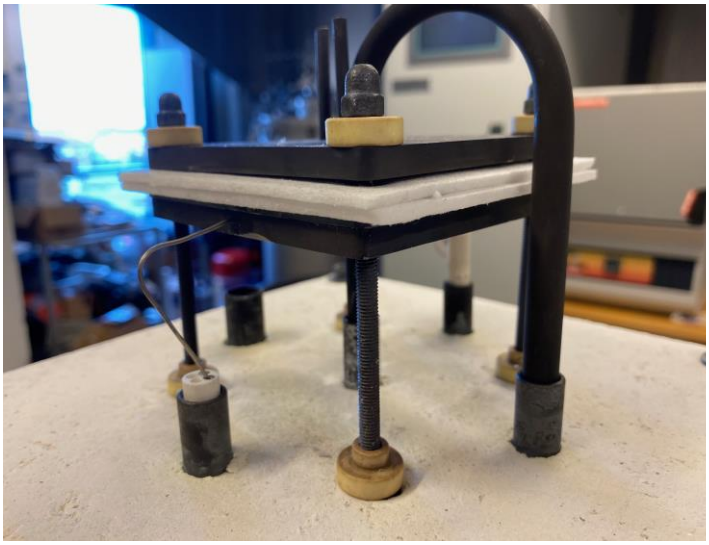

Figure 24 Attached nickel wire in the mounted cell

3.1.4 Mixing of Ammonia

The experiment was conducted using three variants of diluted ammonia solution: 5.9 wt%, 15.2 wt% and 32 wt%. The latter was taken directly from the original bottle seen in Fig 25, while the two weaker solutions were obtained by diluting the original solution with distilled water in 500ml bottles as seen in Fig 26. The concentration on the bottle is given in weight per cent while the dilution was originally blended in term of volume (1:1 and 1:4 ratio between distilled water and ammonia). The calculated concentration in terms of wt% is found in table 10. The volumetric mixture of ammonia solutions and distilled water along with necessary quantities used to calculate the wt% are presented in table X.

Table 10 Overview of ammonia solution and distilled water mixtures.

	15.2% Ammonia solution		**5.9% Ammonia solution**		**Molecular Weight**	**Volumetric Mass Density**
	Volume [ml]	Weight [g]	Volume [ml]	Weight [g]	[g/mol]	[g/ml]
32% ammonia	250	225	100	90	35.05	0.9
Distilled water	250	250	400	400	18.02	1
Total	500	475	500	490		

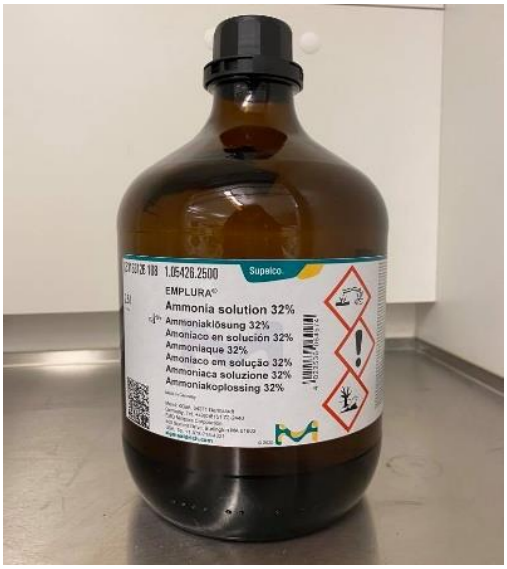

Figure 25 Bottle containing 2.5L of 32 wt% ammonia solution.

Figure 26 Ammonia solution (ammonium hydroxide) diluted to various concentrations with distilled water

3.1.2 Mounting of the Fuel Cell

An overview of each component and the order of placement withing the SOFC is presented in Fig 27 with a corresponding component list found in table 11. Each component is presented along with the amount and a brief comment of their function in the cell. Cutting nickel foam and alumino sheets with the same size as the single cell was done prior to mounting the cell. The cell housing and processing of alumino sheets and nickel mesh can be seen in Fig 28 to 29. Fig 30 to 40 on the following pages displays a step-by-step tutorial of mounting of the cell. Each step consists of a photo and an attached text for explanation.

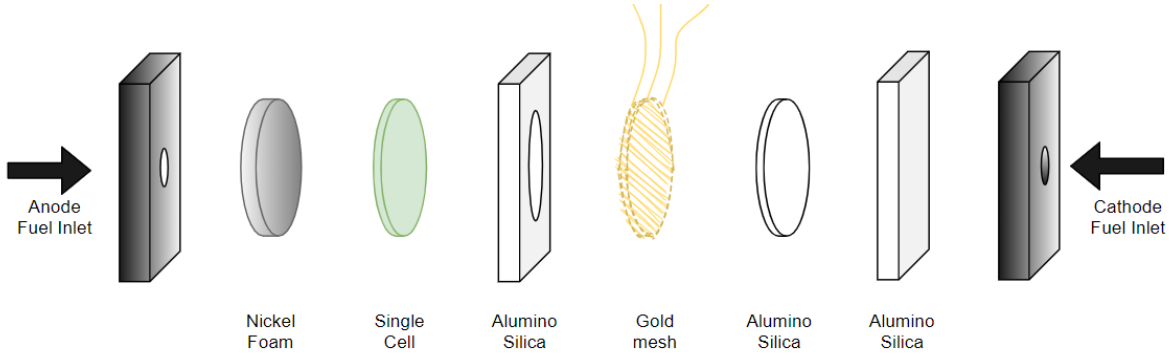

Figure 27 Overview of involved components in the SOFC and their order of placement (not to scale).

Figure 28 Metal flange housings with rods, springs, nuts and stop washers disassembled

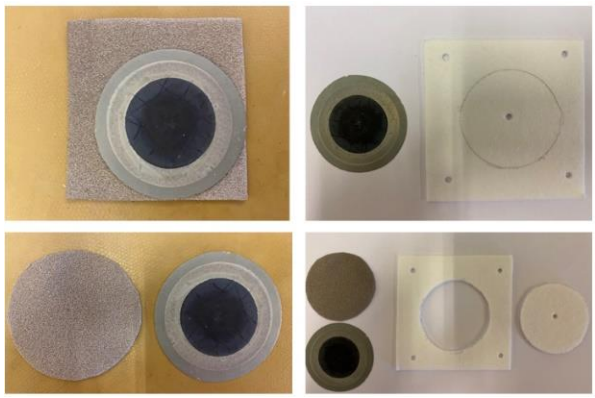

Figure 29 shows the nickel foam and alumio silica insulating sheets

Table 11 SOFC components list

Fuel Cell Components	Amount	Function
Housing top&bottom	1/1	Inlet of reactants, pressing and holding the inside components in place.
Nickel Foam	1	Catalyst for fuel oxidation and ensures good electric connection between anode electrode and anode housing.
Alumino Silica	2	Electric isolation between the anode and cathode.
Gold Mesh	1	Cathode Current Collector
Gold Grid	1	Ensures sufficient connection between cathode and the gold mesh.
Single Cell	1	Anode supported single cell containing Ni/YSZ anode, YSZ electrolyte and LSM cathode.
Springs/rods/nuts/stop washer	4/4/4/4	Tightening the housing and the inside parts to reduce leakage and ensure good electric connection

Figure 30 Empty housing-bottom, fuel inlet

Empty housing bottom part. Fuel is supplied to the anode through the hole in the middle of the plate, while excessive gas is combusted out the sides. A nickel wire to measure the anode potential is welded to the housing but was later drilled in into the side.

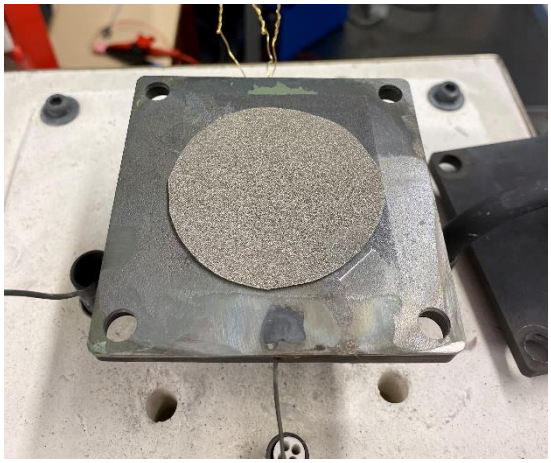

Figure 31 First layer: nickel foam

The first component is a piece of nickel foam with a radius of 25 mm and an original thickness of ~1.5 mm placed on top of the fuel inlet. It is applied to help distribution of fuel in the anode, give good electric connection between the anode electrode and housing, and function as a catalyst improving reaction rates.

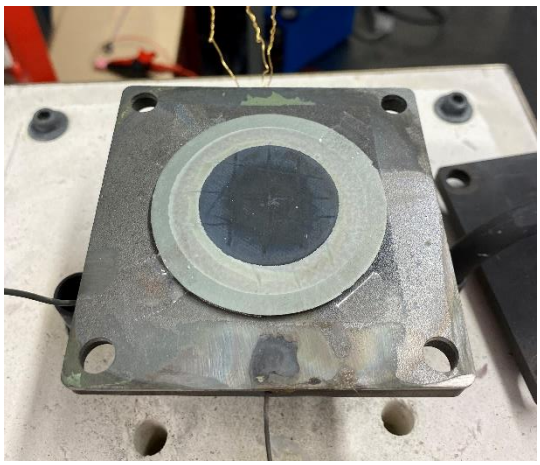

Figure 32 second layer: anode supported single sell

The single cell with radius same as the nickel mesh is placed on top with the anode faced down. The cathode has a radius of 17.5mm and can be seen as the black surface on top. This area corresponds to the active are of the cell.

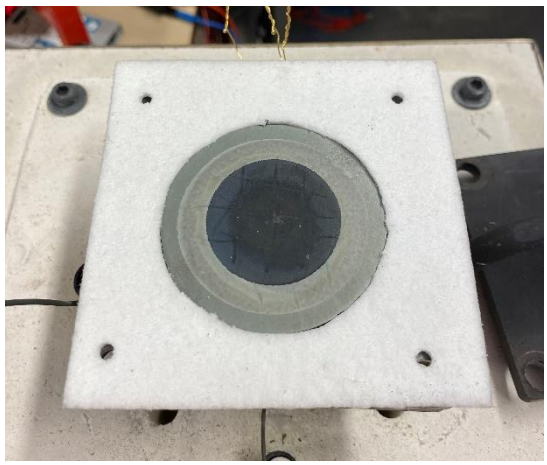

Figure 33 Alumina silica sheet surrounding the cell and nickel foam

Then, a sheet of alumina silica with a carved hole of the same radius as the single cell and nickel mesh is placed. Alumina silica is electrically isolating the anode and cathode to prevent short-circuits.

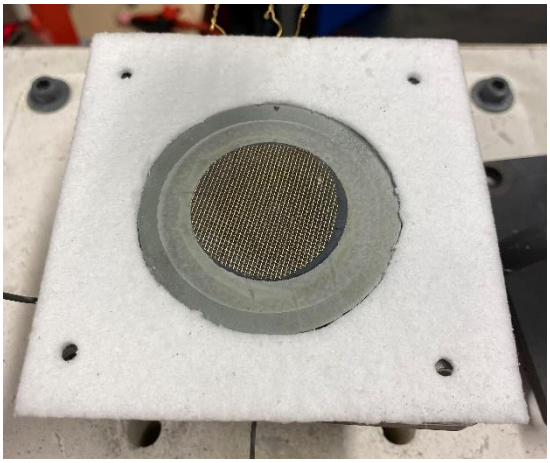

Figure 34 third layer: gold grid

A gold grid is placed on top of the cathode to slightly increase the overall height of the layers to improve the electrical connection between the current collector and cathode electrode.

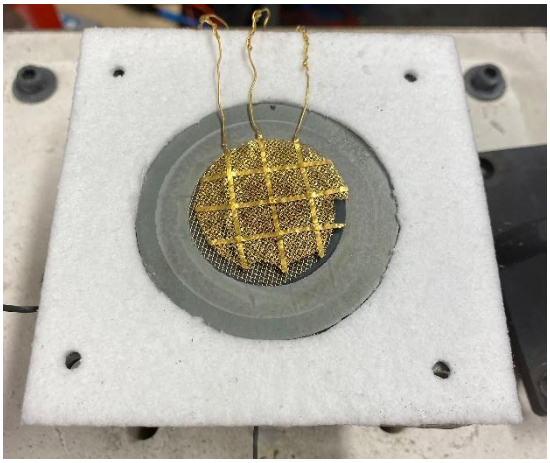

Figure 35 fourth layer: Current Collector made of gold

The current collector in form of a gold mesh with the same radius as the cathode (17.5mm) is placed on top of the gold grid. There are three gold wired connected to the mesh, two to conduct current and one to measure the cathode potential. It is critical that neither of the wires touches the anode while operating the cell as it would result in a short-circuit and damaged components.

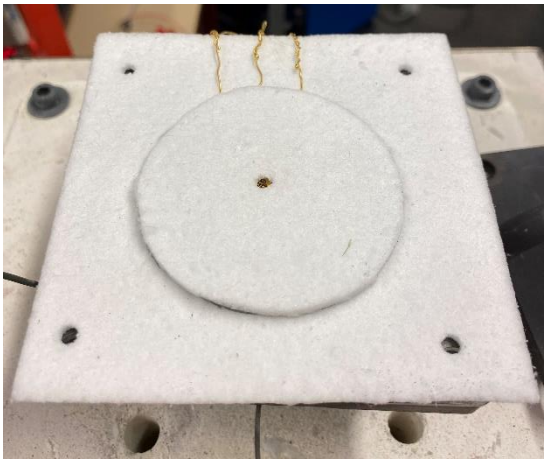

Figure 36 Remaining piece of the first alumina silica sheet

The remaining part of the carved alumina silica is placed on top of the gold mesh.

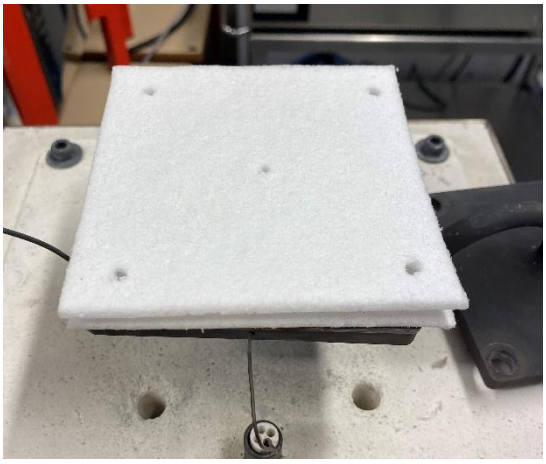

Figure 37 second layer of alumina silica sheet

The electrically isolation between the anode and cathode is ensured by applying another layer of alumina silica.

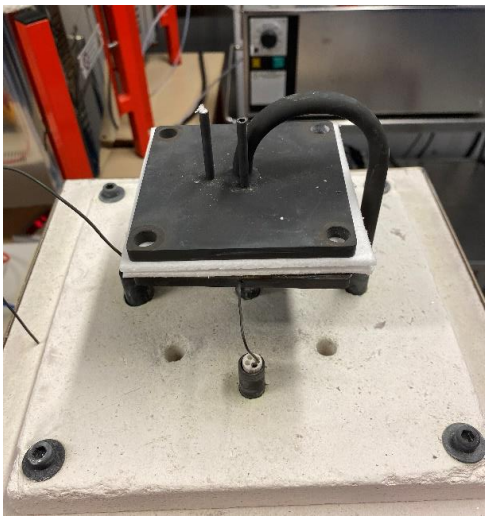

Figure 38 Top of housing in which air is supplied

Top of housing. Air is supplied through the bended pipe in the middle. Thermocouples to measure internal cell temperature is inserted through either of the two smaller pipes.

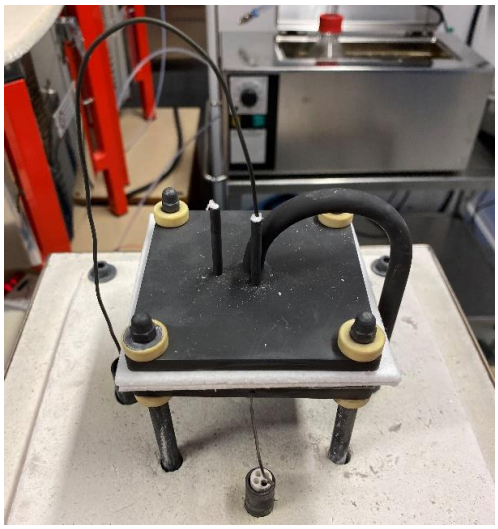

Figure 39 Housing installed with thermocouple and rods to hold it togheter

Complete mounted SOFC. The top of the housing is pressed together by springs on rods compressed approximate 2mm by nuts. A N-type thermocouple is seen as the long bended wire. The thermocouple inlets are plugged by alumina silica pieces to prevent gas from leaking out.

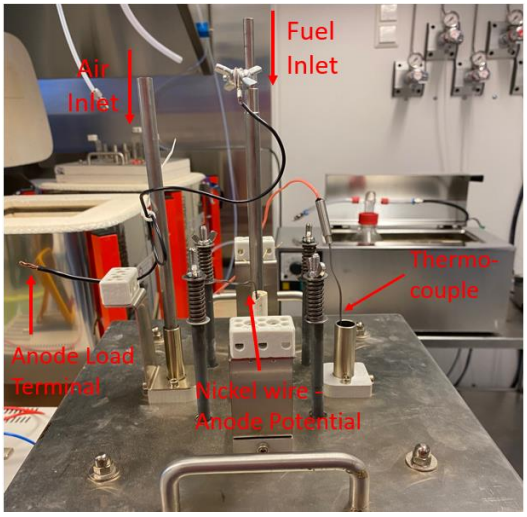

Figure 40 Overview of the top of the fuel cell, marked with fuel inlets and anode terminals. Cathode terminals of the opposite side

On the opposite side of the isolated plate is the rods, springs being compressed by nuts to press the housing together. Reactant gas is supplied through two pipes. Springs, rods, and nuts are used to press the housing parts together. The cathode potential is measured at current collector on the opposite side.

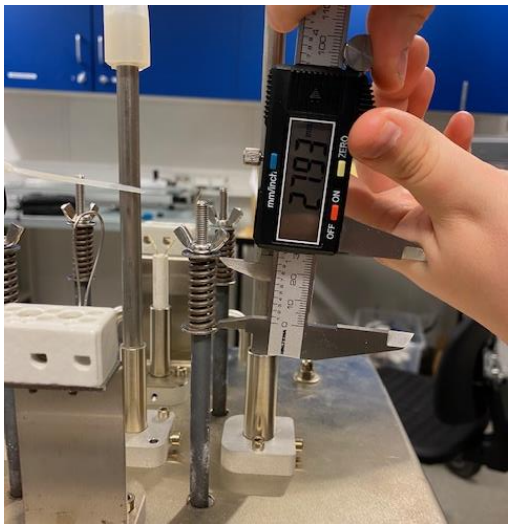

Figure 41 Measuring of spring compression

The force pressing the housing together is a function of compression and spring constant. Too much force could potentially break the cell and must therefore be adjusted carefully. The manufacturer recommended 1-2mm, and a compromise of 1.5mm was used during the experiments.

3.1.5 Experiment Set-up

The lab set-up consists of a SOFC Open Flanges test fixture manufactured by Fiaxell (2), a programmable furnace (1) and various equipment required to operate and monitor the SOFC (3-10). A numbered overview of the lab set-up is seen in Fig 42. The numbers correspond to the numbers in the equipment list found in table 12. The lab set-up was built from scratch and has been gradually improved as the project went on, with great assistance from supervisors and the lab manager.

Hydrogen and nitrogen gas was supplied to the gas outlet valves (3) on the wall through pipes (5-10 bar) from tanks located in a separate room. From the valves the gas pressure is reduced to approximate 2 bar and supplied to the mass-flow controllers (4) who distributes the gas to its intended location (2 or 6). Air was initially supplied from a simple fish-tank air pump but was eventually swapped to a mini-compressor (10) to ensure a more reliable supply. The mass flow of air was not controlled by mass-flow controllers, but more than enough flow was ensured. A table of the gas supplies is found back in table X in chapter 3.1.2. The performance of the cell was tested at various load, simulated by using a power supply (8) in reverse. The voltage was adjusted in steps of 50mV, measured by the multimeter (9), while the current was read directly of the display on the power supply. A N-type thermocouple was used to measure the internal temperature of the cell but had to be measured in mV using a multimeter (7), for then to be recalculated to temperature using tabulated values. The thermocouple used to ensure steady temperature within the cell when moving to new temperatures.

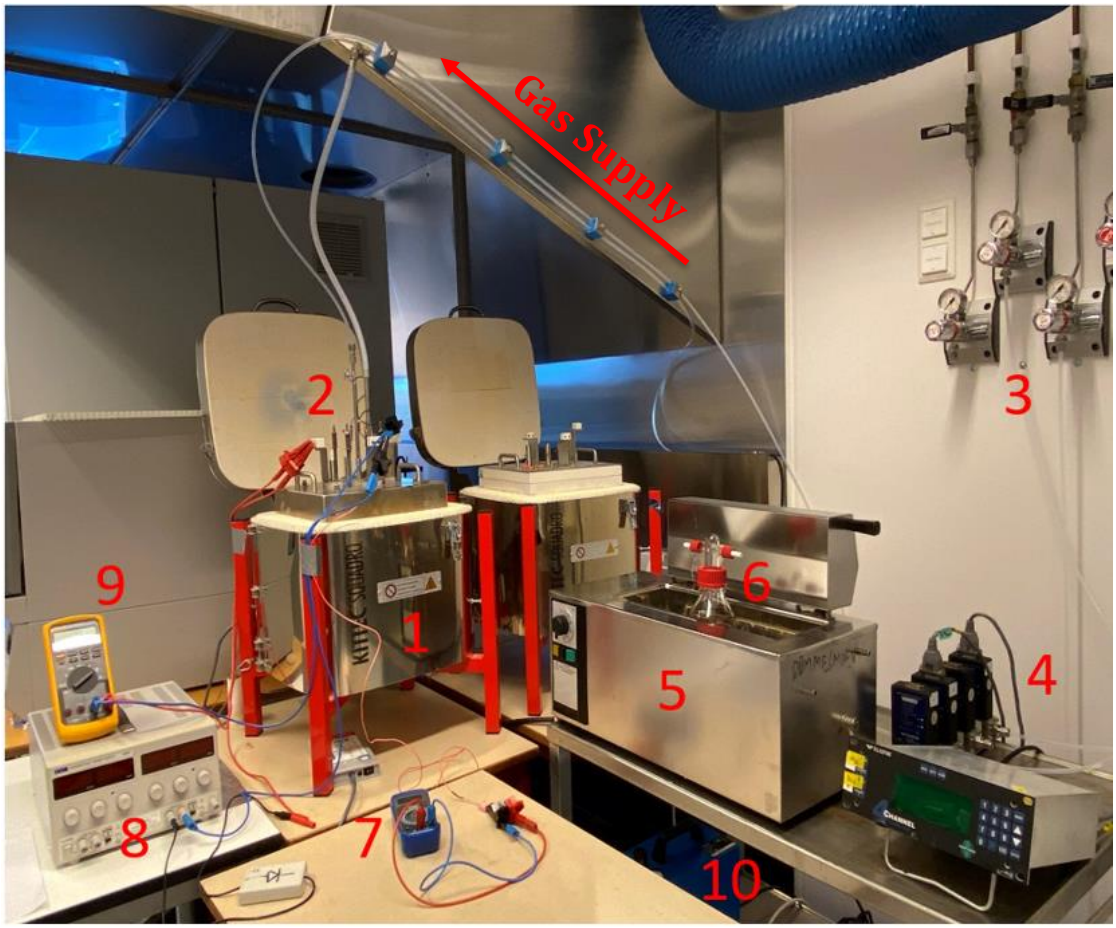

Figure 42 Numbered overview of the lab experiment set-up.

Table 12 List of equipment used in the lab-experiment.

Nr	Equipment	Type
1	Programmable Furnace	Bentrup TC505
2	SOFC	Fiaxell Open Flanges test set-up
3	Gas supply	Hydrogen/Nitrogen
4	Flow Meters	Teledyne
	Flow Meter Controller	Teledyne, 4 channel THPS-400
5	Heating bath	memmert
6	Drechel bottle with ammonia solution	6%, 16% and 32% solutions
7	Multimeter measuring N-type thermocouple	
8	Power Supply (Load) with ammeter	TTi EX354RD Dual Power Supply 280W
9	Multimeter measuring cell voltage	Fluke 87 V Digital Multimeter
10	Air Supply	Mini Compressor MC 90, 90W, 230V
Other		
Diode		
Thermocouple		N-type
Ammonia		32% Ammonium Hydroxide - NH_4 (lq)
Distilled water		-
Drechsel bottle		500ml gas washing bottle - VitraPOR
Measuring cables of various length		
Tubing and Connections		Swagelok connections

3.1.6 Experiment Implementation

A homemade schematic of the set-up operating with the hydrogen/nitrogen mixture or pure hydrogen is presented in Fig 43. The experiment could start when the cell was thoroughly mounted, the furnace heated, and the safety measures and system controlled. The air was always continuously running. Supplying hydrogen to a heated cell without first applying inert gas would likely cause an explosion or combustion harming internal components and potentially cause more severe damage. Therefore, nitrogen had to be supplied by itself for some minutes to remove oxygen from the chamber prior to opening the hydrogen valve. Hydrogen was gradually mixed in until the desired flow rate was reached, after which the nitrogen could be turned off when desired. Excessive gases are combusted out the side of the cell but within the furnace. After testing was all the gas, except air, shut off, but the furnace was often maintained on to spare time. The tubing is slightly changed when the cell is operated with ammonia. Hydrogen is swapped out with ammonia solution in a drechsel bottle washed with nitrogen to a carry ammonia vapor into the anode chamber. In case of spillage or leakage, the lab facilities were sufficiently ventilated, and the heating bath (5) was unpowered but acted as a container in case of spillage. A schematic showing the connection of the pipes is seen below in Fig 44. Nitrogen is washed through the drechel bottle of ammonia solution.

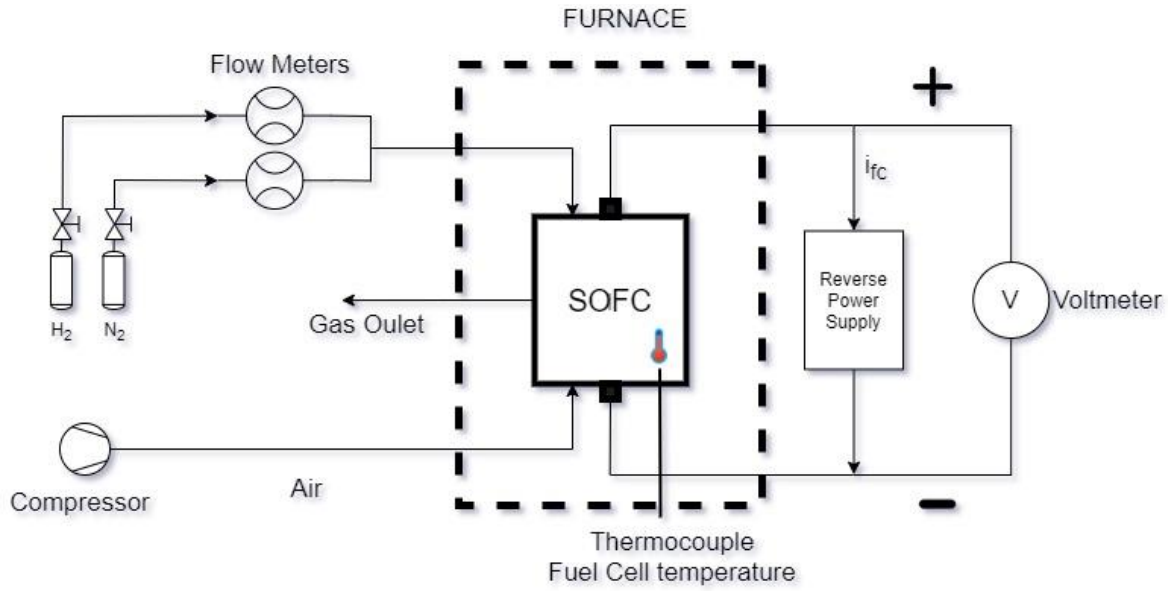

Figure 43 Schematic of the lab-experiment set-up directly fuelled by pure hydrogen or a hydrogen/nitrogen mixture.

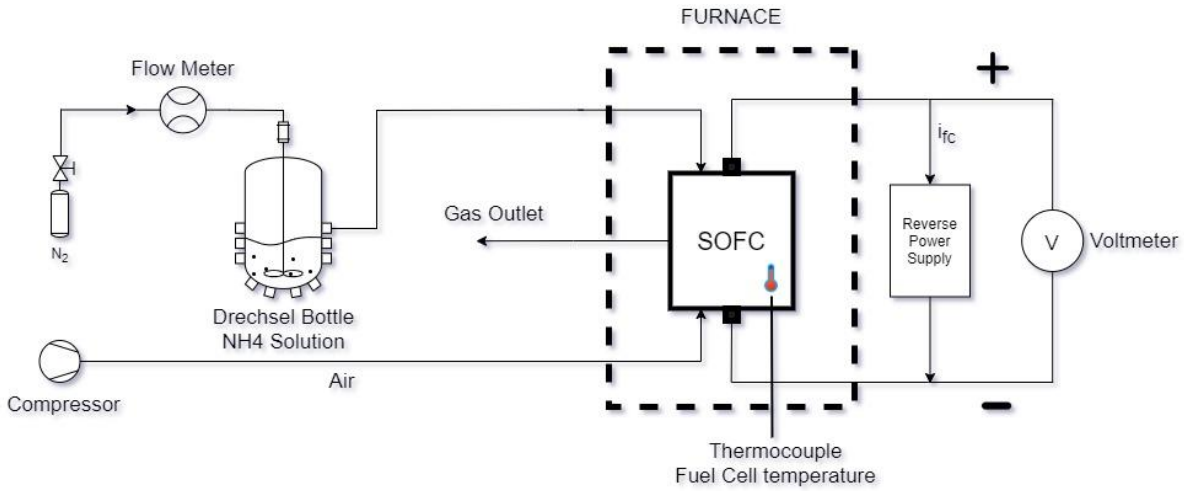

Figure 44 Schematic of the ammonia lab-setup. Nitrogen gas supplied to a drechsel bottle containing an ammonium hydroxide solution, vaporing ammonia gas into the fuel cell.

3.1.5 Risk Assessment

The experiment is conducted using multiple toxic and/or explosive gases heated in a furnace operating at temperatures up to 850°C. It goes without saying that an experiment of this sort involves risks that must be identified, evaluated, and handled to ensure both human- and environment health. The methodology presented in Fig 45 on the following page is developed to ensure a safe work environment before, during and after the start of the project. It is developed using recommendations and guidance from the United States Environmental Protection Agency (EPA)[48], relevant datasheets and user manuals, and guidance from experienced users of the chemicals and equipment involved in the experiment.

Risk is defined by two dimensions: the probability of an accident to occur (1), and the associated consequences (2). Table 13 and 14 presents a 3x3 risk assessment matrix developed to evaluate the various activities performed during the lab experiment. All potentially hazards to human and environmental health are given a probability and consequence rating resulting in an overall risk rating, presented by the risk assessment matrix. Activities evaluated to the yellow or red risk level requires risk management to reach a tolerable level (green level of risk) before they can start. Risks is handled by implementing safety measures to either reduce the probability of an accident, reduce the consequence of an accident, or a combination of both. The risk evaluation of the lab experiment is found in table 15 in the following pages.

Table 13 Risk assessment matrix used for risk rating of activities conducted throughout the experiment.

			Probability		
			Unlikely	Potentially	Likely
			1	2	3
Consequence	Minor injury	1	1	2	3
	Major injury	2	2	4	6
	Critical injury	3	3	6	9

Table 14 Risk rating score explanation.

1-2	**Low risk** - Tolerable, activity can be conducted
3-4	**Medium risk** – Simple safety measures required prior to activity start.
6-9	**High risk** - Do not start activity, thorough evaluation and safety measures must be implemented prior the start of the activity

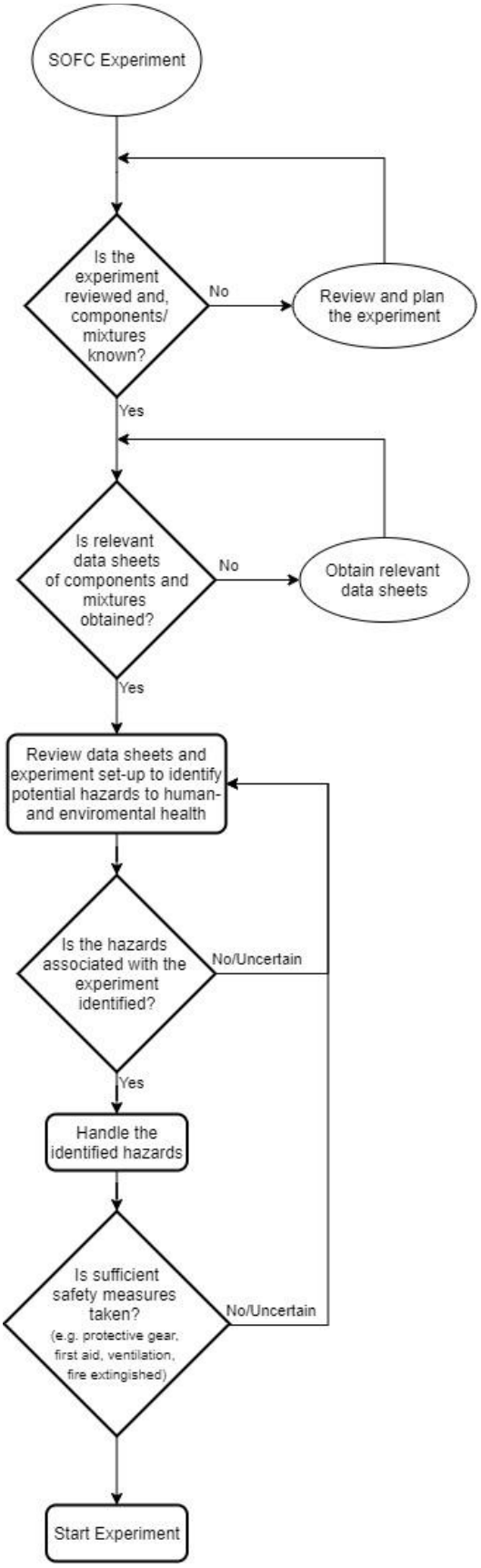

Figure 45 Risk Assessment flow diagram

Table 15 provides an overview of the risk analysis of the lab experiment activities causing any danger to human- or environmental health. Each activity is evaluated by collecting information from relevant datasheets and/or user manuals, as well as discussions with experienced users of the various substances and equipment. The risk rating was first evaluated independent of safety measures to give a clear picture of the underlaying risk of each activity. Necessary safety precautions were then implemented, and a new risk rating was evaluated to ensure a tolerable level of risk for the entirety of the lab experiment.

Table 15 Risk evaluation of the lab experiment activities

Activity	Potential Hazard	Who is at risk	Risk Rating			Risk Management	New Risk Rating		
			P*	C**	R***		P*	C**	R***
Use of ammonia	Leakage/spoiling leading to human and environmental exposure	People walking in and out of the lab, environment.	2	3	6	Leak testing, safety glasses, protective gloves and clothing, sufficient ventilation, examine datasheet	1	2	2
Use of Hydrogen	Explosion if used directly at high temperatures without inert gas.	People in close approximation of the set-up	1	2	2	Follow user manual, ensure that inert gas is always applied first and slowly increase hydrogen flow.	1	2	2
Use of Nitrogen and Argon	Replacing surrounding oxygen causing suffocation	People in close approximation	1	2	2	Ensure sufficient ventilation	1	1	1
Use of furnace operating up to 850°C	Burns of human, ignition of materials/gases may cause fire (explosive gas-tanks in the room next door)	People in the building and the building/lab itself	2	3	6	Be observant and make sure the furnace area is free for combustible materials, fire extinguisher in close approximation	1	2	2

* P = Probability of accident

** C = Consequence of accident

*** R = Total risk of accident

3.2 Modelling

An electrochemical model of the SOFC operated by hydrogen was developed to estimate fuel cell parameters such as activation energy and exchange current. Enthalpies and Entropies was calculated in a regular excel sheet by applying the equations presented in chapter 2.4 to tabulated thermodynamic quantities found in textbooks about thermodynamics [8],[38], [39].

A homemade MATLAB script was developed to model the SOFC polarisation losses and plot the polarisation curve. Many fuel cell parameters are not easily obtained without extensive experimental work, and numerous parameters used in this report is adopted based on parameters found in relevant paper [34], [35], [36]. Adjustments of the activation energy and pre-exponential values were made to fit the modelled curve with the experimental results, as they seemed to have the highest impact on the performance. A parameters list can be found in the table 16. Values without reference is either obtained by calculations, assumptions or are known operating parameters.

Table 16 Parameter list of developed SOFC model fuelled by hydrogen.

Cell and Operational Parameters	**Value**	**Ref**
Open Circuit Potential E_{rev} [V] (Hydrogen)	1.10	
Cell radius r [m]	0.0175	
Operating Temperature T [K]	1048.15 (750°C)	
Operating Pressure p [bar]	1	
Electron transferred pr. reaction z	2	
Transfer coefficient α	0.5	
Anode Exchange Current i_{0_a} [A/m²] (calculated)	1150	
Cathode Exchange Current i_{0_c} [A/m²] (calculated)	98.6	
Electrode Porosity ε	0.3	[37]
Electrode Tortuosity ζ	6	[37]
Average pore radius r [m]	5e-7	[37]
Anode		
Anode thickness τ_a [m]	200e-6	
Conductivity σ_a [S/m]	80e3	[37]
Pre-exponential coefficient b_a	6.5e11	
Activation Energy E_{act_a} [kJ/mol]	153.5	
Kinetic Volume Hydrogen v_{H2} [m³/mol]	6.12e-6	[36]
Kinetic Volume Oxygen v_{O2} [m³/mol]	16.3e-6	[36]
Kinetic Volume Steam v_{H2O} [m³/mol]	18.5e-6	[36]
Electrolyte		
Electrolyte thickness τ_c [m]	40e-6	
Conductivity σ_{el} [S/m]	$33400e^{\frac{-10.3*10^{-3}}{T}}$	[34]
Cathode		
Cathode thickness τ_c [m]	50e-6	
Conductivity σ_c [S/m]	8.4e3	[37]
Pre-exponential coefficient b_c	2.35e11	[43]
Activation Energy E_{act_c} [kJ/mol]	159	[43]

4 Results

This chapter presents the results of the experimental and modelled work done throughout this project, meanwhile the discussion awaits in chapter 5. The results are presented in two parts: comparison of the three ammonia concentrations at 750°C (1) and 32wt% ammonia concentration, compared to hydrogen, and the hydrogen/nitrogen mixture at 600°C to 850°C (2). This is due to difficulties of comparing results due to significant change in performance during the many hours of operating the cell. The results in part one is therefore better than the ones in part two.

4.1 Experimental Results

4.1.1 Part One –Ammonia Concentrations at 750°C

Fig 46 and 47 presents the polarisation- and power curves of the SOFC operating at 750°C with 32wt%, 15.2wt%, and 6wt% ammonia solution vaporized at 20°C and carried by a flow of 200 ml/min of nitrogen washed through a drechel-bottle. The maximum power density ends at 45 mW/cm^2, 37.5mW/cm^2 and 22mW/cm^2 respectively. From the plot it is seen an increased performance of the two stronger solution, while it seems like the 5.9% solution suffers from mass-transfer losses as the curve cuts steeper at approximate 50mA/cm^2.

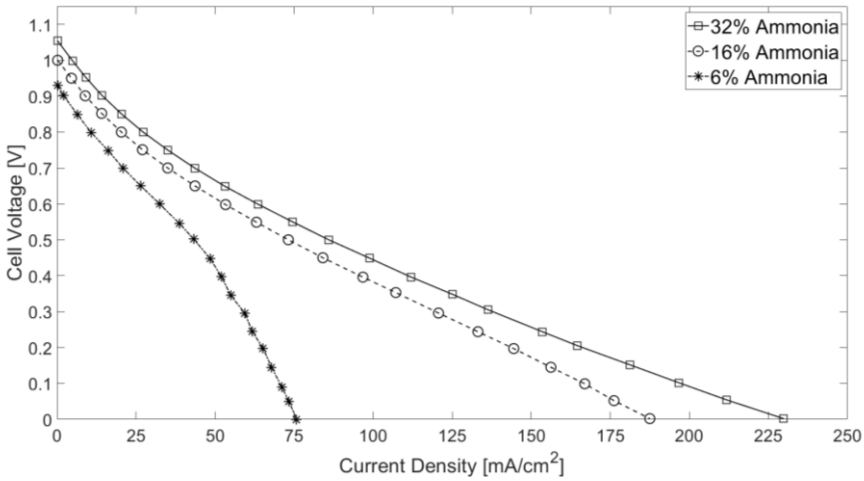

Figure 46: I/V-curve of the SOFC fuelled by 5.9wt%, 15.2wt% and 32% ammonia concentration at 750°C.

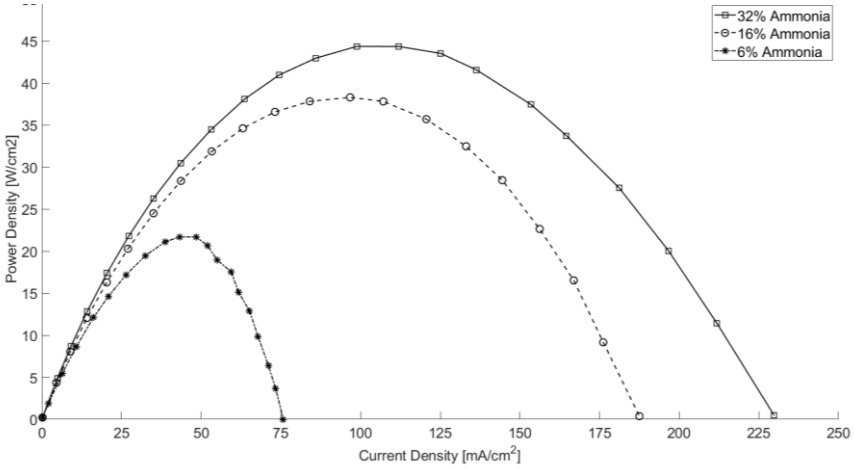

Figure 47 Power-density curve of the SOFC fuelled by 5.9wt%, 15.2wt% and 32wt% ammonia solution at 750°C.

4.1.2 Part Two – Comparison of Ammonia, Hydrogen and Hydrogen/Nitrogen

In this section is 32% ammonia concentration, hydrogen, and the hydrogen/nitrogen mixture presented in the mentioned order as the temperature is gradually increased from 600°C to 850°C. The first plots seen in Fig 48 and 49 displays the I/V- and power density curves of the 32% ammonia solution as the temperature was increased in steps of 50°C. It can be seen a nonlinear increase in performance as the temperature increases.

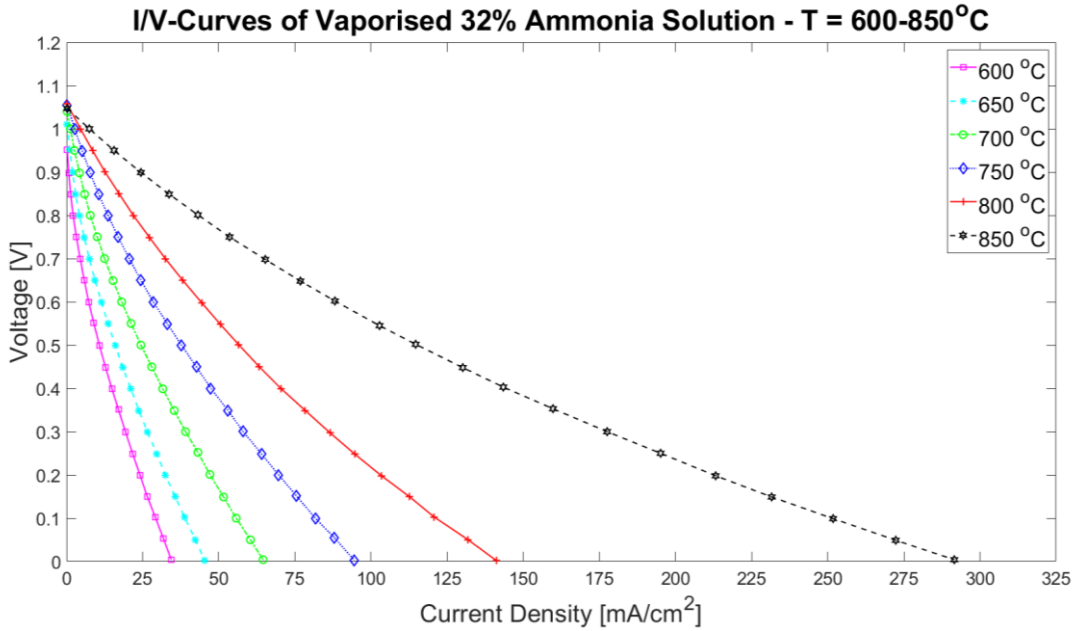

Figure 48 I/V-curve of SOFC fuelled by vaporized 32% ammonia solution.

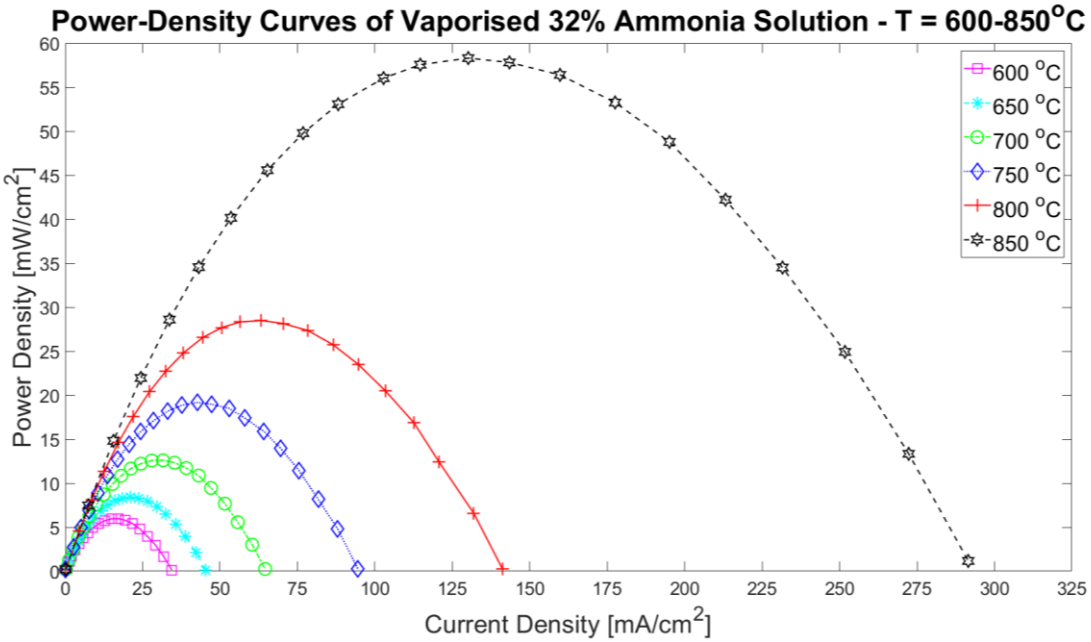

Figure 49 Power Density Curve of SOFC fuelled by vaporized 32% ammonia solution.

The plot in Fig 50 and 51 presents the performance of the SOFC fuelled by pre-cracked ammonia, simulated by supplying a mixture of H_2 and N_2 at a rate of 3:1. More than sufficient flow rates were used prevent the occurrence of mass-flow losses.

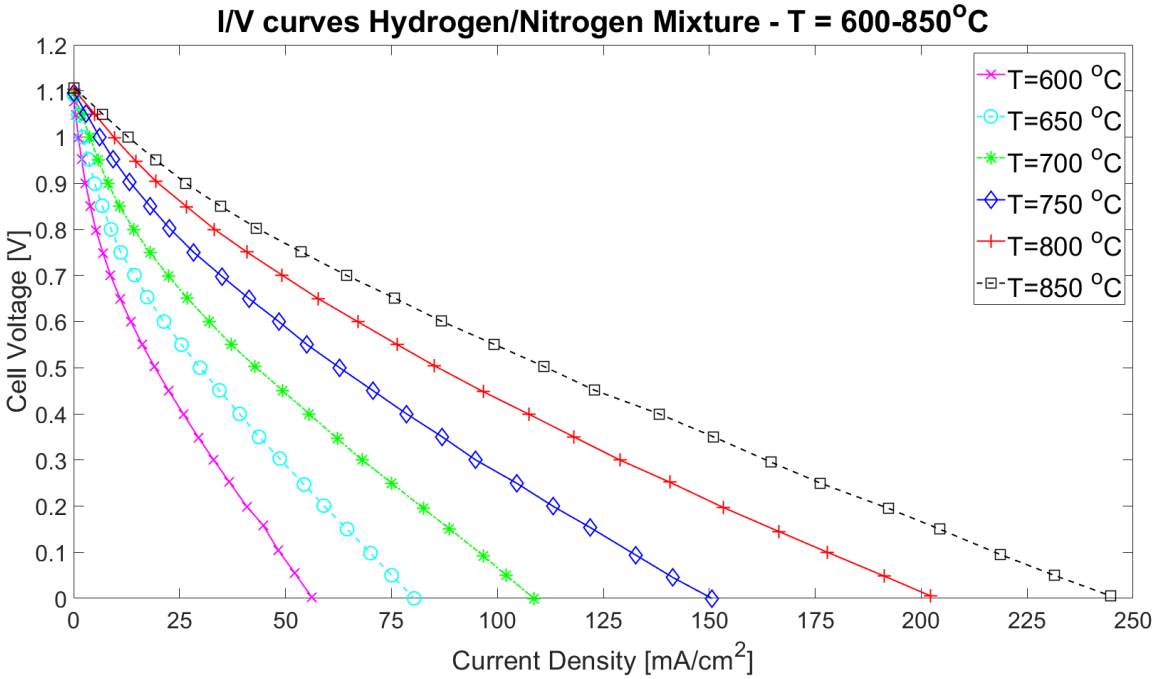

Figure 50 I/V-curve of SOFC fuelled by a 3:1 mixture of hydrogen and nitrogen.

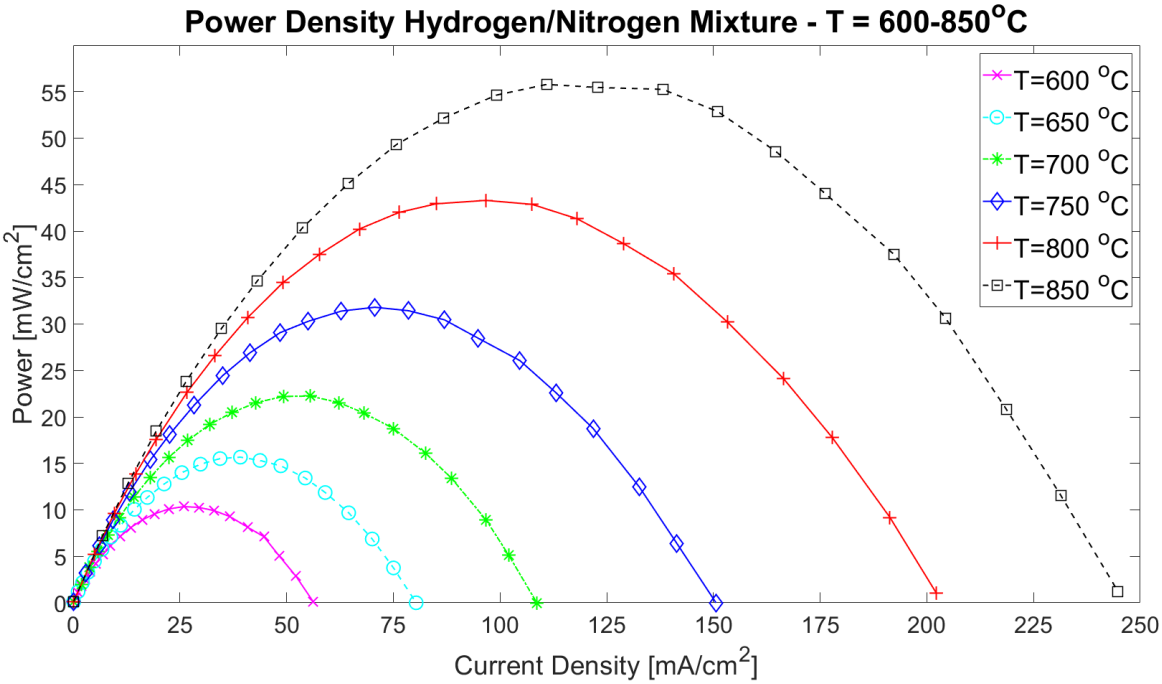

Figure 51 Power Density-curve of SOFC fuelled by a 3:1 mixture of hydrogen and nitrogen.

The plots in Fig 52 and 53 displays the I/V-curves and power-density curves of the SOFC fuelled by 566 ml/min of pure hydrogen at various temperatures.

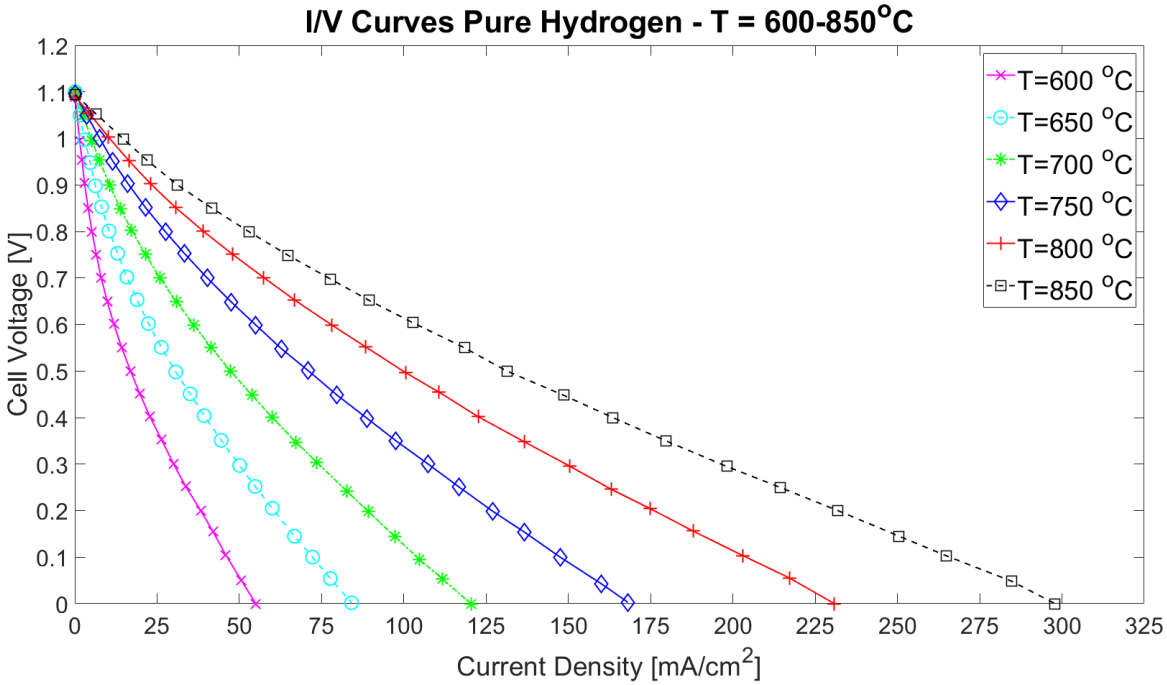

Figure 52 I/V-curve of SOFC fuelled by pure hydrogen.

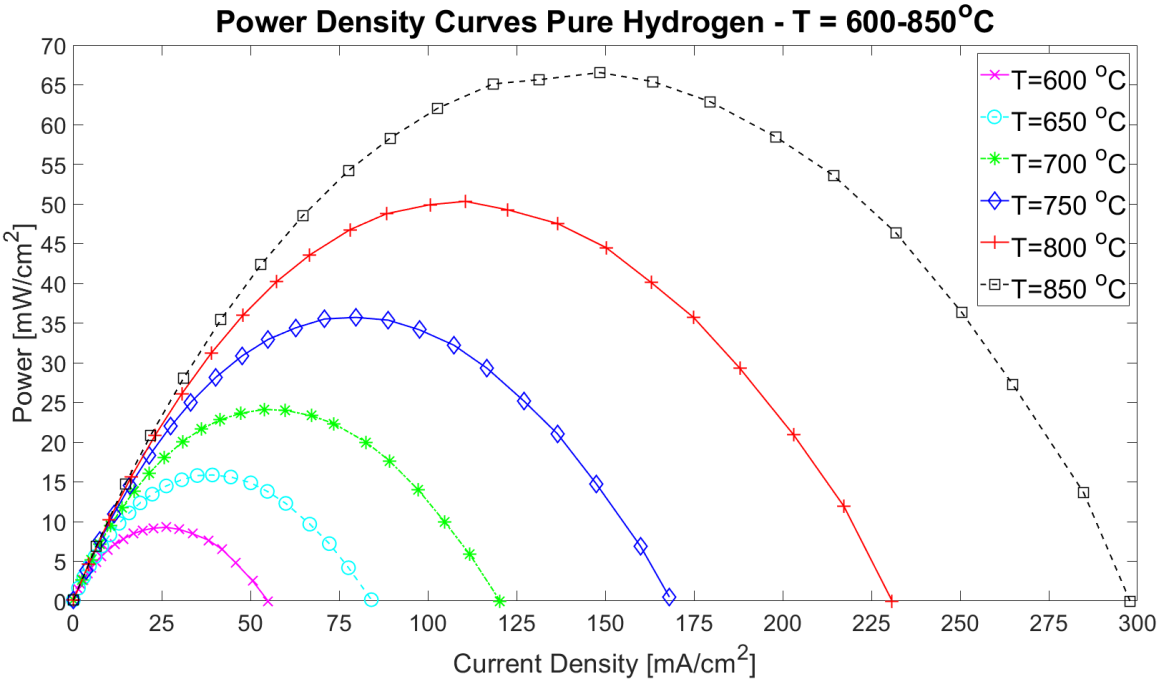

Figure 53 Power Density-curve of SOFC fuelled by pure hydrogen.

The plots in Fig 54 to 56 combines the I/V and power density curves of 32wt% ammonia, hydrogen, and hydrogen/nitrogen mixture at 650°C, 750°C and 850°C. An interesting result is the significant increase at 850°C where ammonia perform equally and even better than the hydrogen/nitrogen mixture. It should also be noted that the rightmost y-axis is scaled to best fit the results.

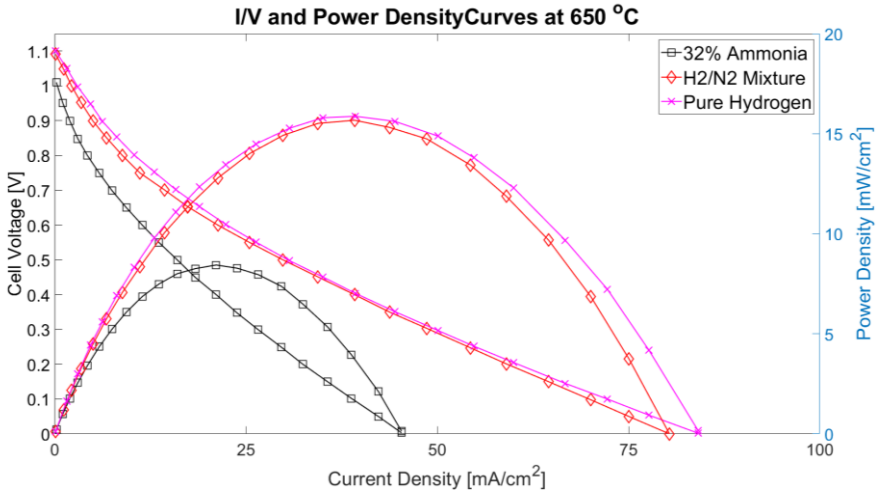

Figure 54 Combined I/V- and power density plot at 650°C.

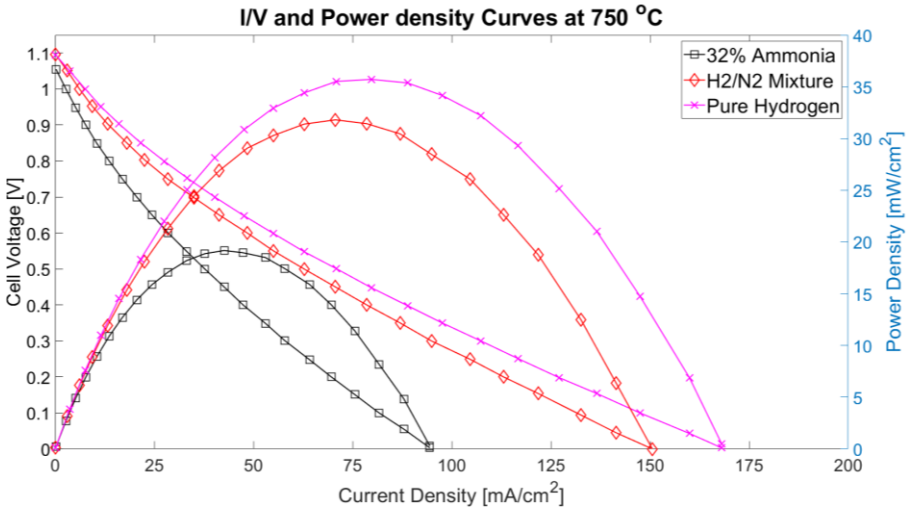

Figure 55 Combined I/V- and power density plot at 750°C

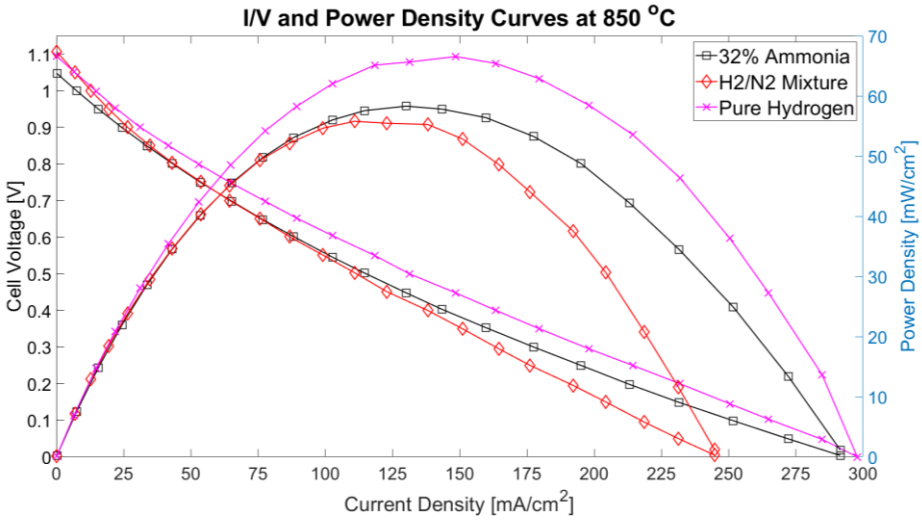

Figure 56 Combined I/V- and power density plot at 850°C.

Fig 57 to 59 presented the OCV, maximum power density, and calculated ohmic resistance of the results seen in the previous sub-chapter. The experimental ("Exp", solid line) OCV results is plotted along with theoretical calculated values ("Model", dotted lines), based of thermodynamic calculation done in excel.

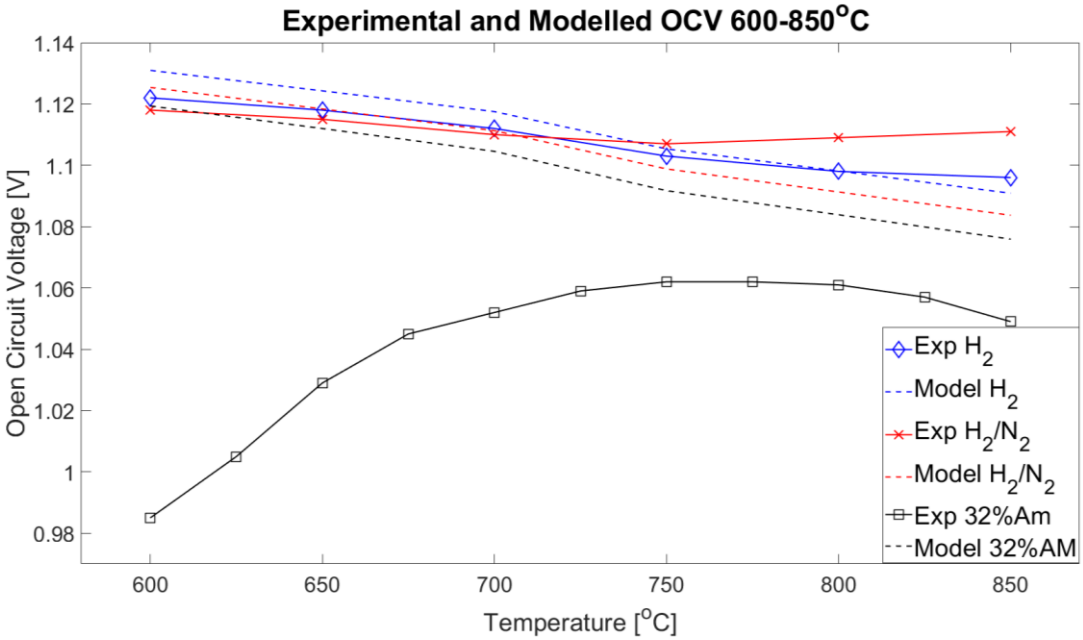

Figure 57 Open Circuit Voltage Comparison of fuels at increasing temperatures

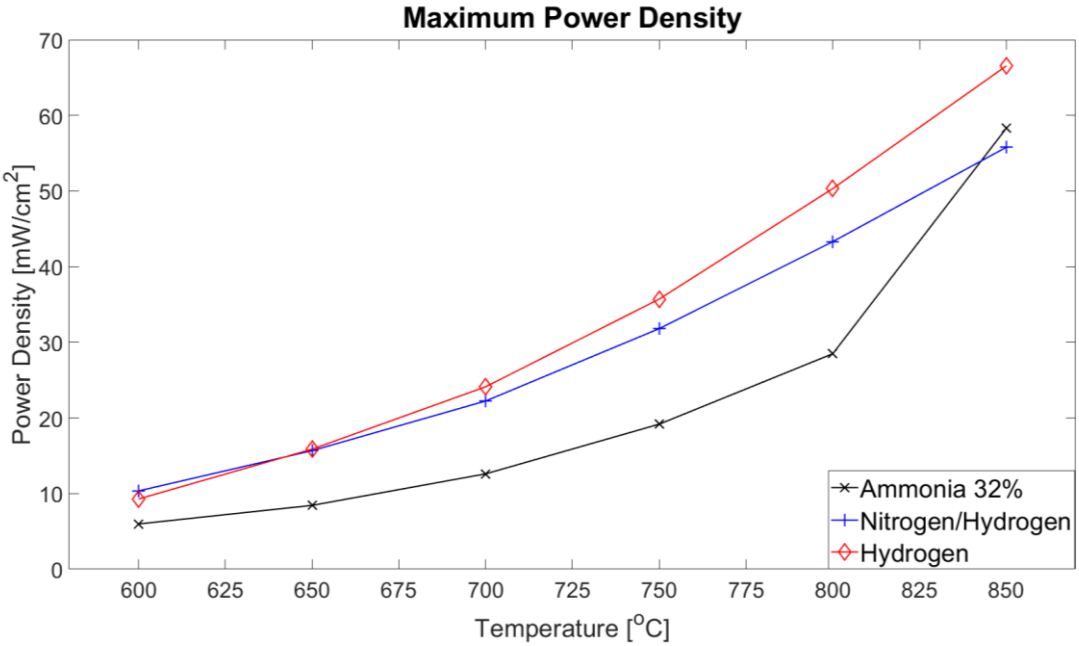

Figure 58 Maximum Power Density at increasing temperatures

Fig 59 display the ohmic resistance in the cell while operating with 32% ammonia, hydrogen, and hydrogen/nitrogen at increasing temperatures. The resistance is estimated by analysing the slope of the linear mid-section of the I/V curves. A clear indication of reduced ASR can be seen at the temperature is increase.

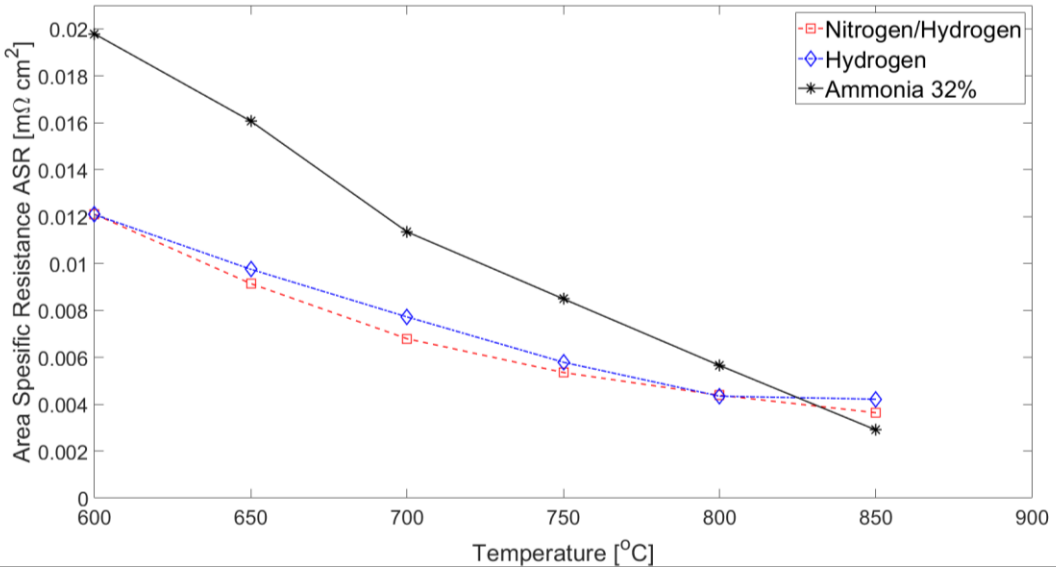

Figure 59 Calculated Cell Resistance

4.1.7 Single Cell Condition

Fig 60 displays the cell after weeks of testing. The leftmost picture shows the cathode and current collector as the housing was dismantled. At this point the cell was still whole and seemed unharmed. When it was attempted removed it became clear that the cell was fused to the underlaying nickel foam, and therefore unable to be retrieved in one piece. As seen in the rightmost picture, the cell broke into five pieces during the removal due and the missing part is that got stuck to the nickel foam. Black marks are also marking that was not initially there.

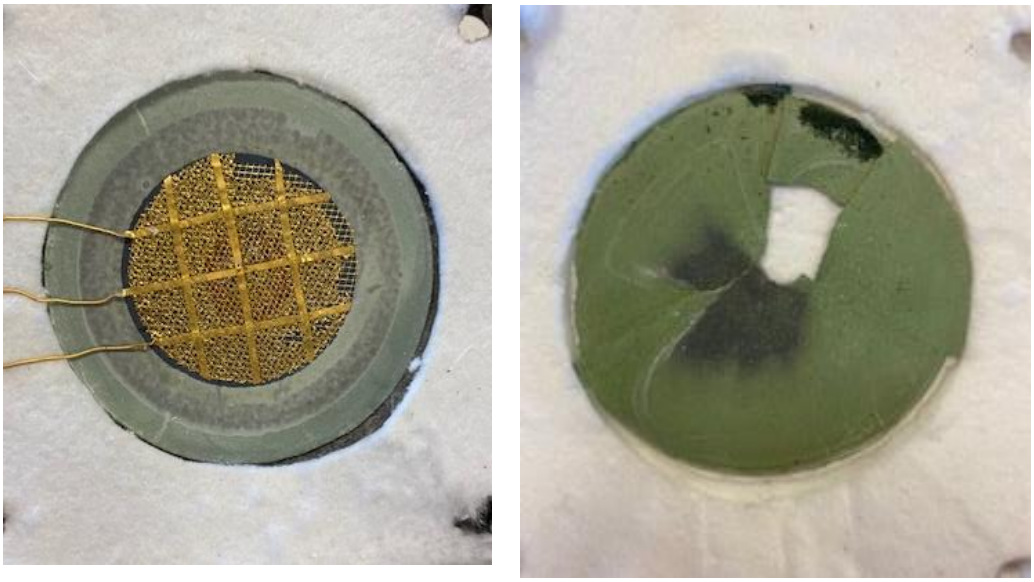

Figure 60 Shows the single cell after testing. In the leftmost photo the cell is still in one piece and not attempted removed. The rightmost photo shows the cell after it was removed and cracked into 5 pieces.

4.2 Modelling Results

A mathematical model of the SOFC fuelled by hydrogen was developed using excel to calculate thermodynamics quantities and MATLAB script to simulate the polarization losses as the current increases. The plot includes the experimental obtained polarisation curve from of hydrogen at 750°C found in Fig 61, the fitted polarisation curve from the model, calculated activation losses for anode and cathode, ohmic losses and diffusion losses (almost negligible). Parameter list is found back in chapter 3.2.

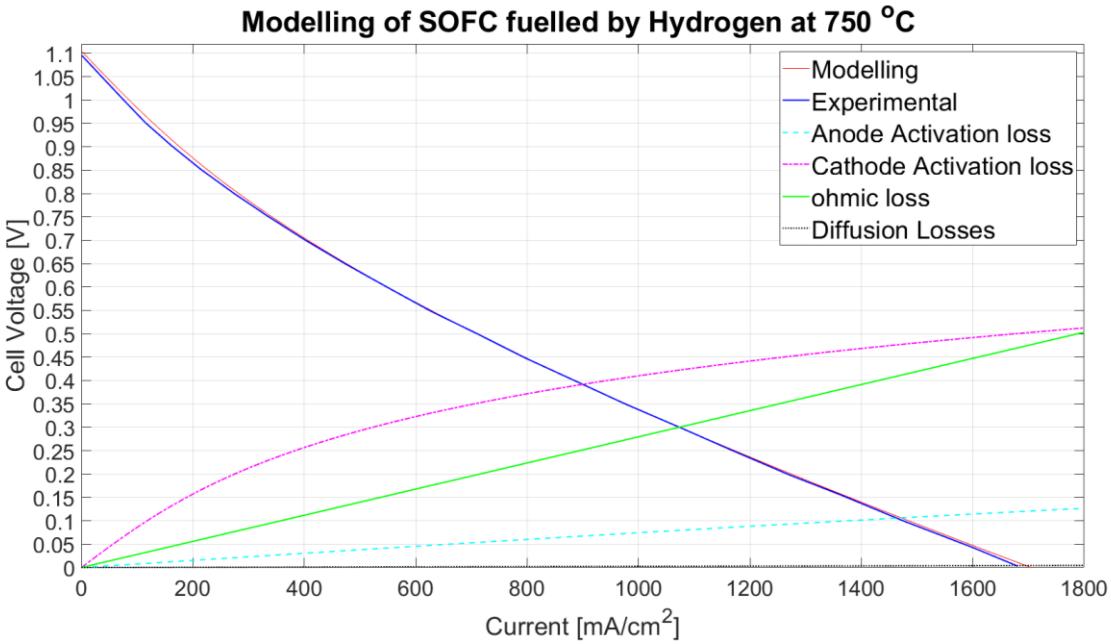

Figure 61: Modelling results of the SOFC fuelled by Hydrogen.

5 Discussion

The objective of this study is to investigate the feasibility of ammonia as an alternative fuel in SOFC systems. An experimental work was conducted with a planar anode supported single cell composed by Ni/YSZ anode, YSZ electrolyte and LSM cathode at temperatures ranging of 600°C to 850°C in an Open-Flange test set-up. The cell was fuelled by 5.9wt%, 15.2wt% and 32wt% vaporised ammonia concentration and a simulation of pre-cracked ammonia in form of a mixture of nitrogen and hydrogen. Pure hydrogen H_2 was also tested to act as a reference to the performance of the rest.

Abundance supply of fuel was used in scenarios without ammonia, to an extent where the fuel utilisation could be approximated to 0%. Because the cell is an unsealed open flange will a significant amount of unreacted gas combust out the sides. Nevertheless, the objective of the experiment was not to develop an efficient and commercial attractive cell, but to investigate the feasibility of ammonia. Supplying huge amount of fuel makes the mass-transfer losses almost negligible, while the activation- and ohmic losses remains to shape polarisation losses. Exceptions of mass-transfer losses is however seen in Fig 46 by the 5.9wt% and 15.2wt% ammonia concentrations at approximate 50mA/cm^2 and 150 mA/cm^2 respectively, indicated by the increase of slope.

The experiment showed great performance of aquatic ammonia solution as fuel in the cell. Especially at higher temperature was the performance surprisingly good, showing even better results than to the ones of pre-cracked ammonia, and very well comparable to the results of pure hydrogen. The general impression of the performance of ammonia insinuates that ammonia can be a feasible alternative of fuelling SOFC systems. A significant increase of maximum power density was observed when going from 800 to 850°C which is explained by an almost exponential correlation between the catalytic activity of the endothermic cracking and temperatures. It was however not expected to equally good results as the simulated pre cracked ammonia due to the presence of steam from the aquatic solution. Decent results of ammonia were also presented at lower temperatures but somewhat lower. This was expected due to the reduced cracking activity and thereby a lowered hydrogen partial pressure.

Comparing the results in part one with part two indicates that the cell has been exposed to unintentional changes of either cell properties or operating conditions during the project. Both the 16wt% and 15.2wt% ammonia concentrations in part one achieved higher maximum power densities than hydrogen in part two at the same temperature. This is most likely caused by either cell degradation or a change in operating conditions. Mass-transfer loss due to insufficient supply of fuel is a possibility, but this would likely be seen as an increased slope at the polarisation curve. Assuming the flow rate is intended, the supply would be many times the required minimum, even to an extent where the fuel utilisation can be approximated to 0%. It is therefore more likely caused by other parameters such as increased contact resistance due to sloppy tightening of the housing or degradation of the single cell itself. The single cell was taken out of the fuel cell at the end of the experiments showing black burn marks at the anode as seen in Fi. The cell was originally in one piece when the housing was opened but broke into five pieces when attempted removed because it was fused with the nickel mesh layer. The cause could potentially be a significant temperature increase due combustion within the cell. Nitrogen was used as inert gas to prevent combustion, but the time used to reconnect the tubing from the

nitrogen outlet to the ammonia bottle (1-2 minutes) could potentially be long enough for oxygen to find its way back into the cell, but it is all guessing.

5.2 Part One - Ammonia Concentrations at 750°C

5.2.1 OCV

Fig 46 and 47 found in the first section of the result chapter compares the I/V- and power-density curves of each ammonia concentration at a temperature of 750°C. The concentrations of the solution are clearly affecting the partial pressures, seen by the OCV dropping from 1.05V to 1.00V to 0.95V as the concentration decreases. The effect of partial pressure on the OCV is explained by Nernst's equation. The drop of partial pressure is most likely caused by either incomplete cracking of ammonia or a shortage of ammonia supply. Similar studies have showed complete decomposition of ammonia at temperatures in the range of 750°C over nickel catalyst[49], [10] and is therefore considered unlikely. Having said that, the vapor (partial) pressure of ammonia, and thereby hydrogen, are correlated to the temperature and concentration of the ammonia solution. Solutions with lower concentration has naturally a lower partial pressure of ammonia and thereby a mass flow into the cell. A method to increase the supply rate of ammonia is therefore to either increase the temperature or concentration of the solution. Investigating the effect of putting the bottle of ammonia concentration in a bath of hot water or similar measures to increase the temperature is recommended in further works. Another potentially more desirable alternative is to supply pure ammonia gas directly to the cell, but this would require strict safety measures due to the toxicity of ammonia. The lab facilities of this experiment hope to implement such a system but is still in the phase of planning.

5.2.2 Polarisation Losses and Power Density

The first 3/4 of the polarisation curve of the 32% and 15.2% ammonia solutions is close to identical with a slight offset of approximate 0.05V, likely caused by the difference in partial pressure mentioned in the previous chapter. From 50 mA/cm^2 to 150 mA/cm^2, the curve has a clearly linear shape, indicating that ohmic losses is the dominating polarisation loss. However, just as the current passes the 150mA/cm^2, the slope angle of the 15.2wt% solution becomes slightly steeper, meaning the mass-transfer losses starts to have more significant impact on the performance. This indicates an insufficient supply of hydrogen fed to the reaction causing it to slow down. This effect is also seen almost immediately in the 5.9wt% solution curve as well, indicating that the supply is only sufficient to operate the cell at very low currents densities. The maximum power densities of 32wt%, 15.2wt% and 5.9wt% reached 44mW/cm^2 at 110mA/cm^2 and 38mW/cm^2 at 100mA/cm^2 and 22mW/cm^2 at 50mA/cm^2. These results are comparable to those obtained by A. Fuerte et al. [28] who achieved 35mW/cm^2 at 78mA/cm^2 at 700°C using pure ammonia to fuel a tubular cell composed by similar materials as ones used in this project. In comparison to the results of hydrogen and nitrogen obtained in part 2, the maximum power density is 20.5% and 27.3% higher using ammonia in part 1, indicating that the cell parameters have changed.

5.3 Part Two – Comparison of Ammonia, Hydrogen and Hydrogen/Nitrogen

Fig 48 and 49 presents the I/V- and power density curves of 32% ammonia solution, hydrogen/nitrogen mixture, and pure hydrogen presented separately as the temperatures is increased from 600°C to 850°C. All three fuel scenarios show significant improvements as the temperature increases due to the increased reaction rates and electrolyte conductivity. It was discussed back in chapter 2.3.3 the challenges of YSZ at lower temperatures, and a change from 600°C to 700°C increases the conductivity by seven to nine times according to the graph in Fig 12. These results substantiate the topic discussed about YSZ-based SOFC having issues with high ohmic losses at lower temperature due to the very temperature sensitive conductivity. Estimation on inherent resistance of the cell is calculated and plotted in Fig 59. The results shows that the resistance in almost linearly decreasing as the temperature increases, which fits well if compared to the graph found in chapter 2.3.4 showing the conductivity of YSZ aa a function of temperature.

In chapter 5.3.1 to 5.3.3 is the results of each individual scenario discussed. Then in chapter 5.3.4 is the discussion the results compared by looking at similarities, differences, and the reasons behind.

5.3.1 32wt% Ammonia Concentration - 600°C to 850°C

32wt% ammonia was tested at various temperature starting at 600°C. At lower temperature is it clear that the fuel cell performance is exposed to unfavourable cracking activity. This is substantiated by the almost exponential increase of power density at the temperature goes up, giving more favourable conditions for the cracking process. An especially big jump of approximate 30mW/cm^2 in made from 800°C to 850°C, resulting in a maximum power density of 57mW/cm^2. This value is comparable to the ones of hydrogen and hydrogen/nitrogen, meaning approximate complete cracking of ammonia can be assumed.

5.3.2 Hydrogen and Nitrogen Mixture - 600°C to 850°C

Pre-cracked ammonia was simulated using hydrogen and nitrogen supplied at a 3:1 rate. This led to a somewhat linear behaviour of the maximum power densities at increasing temperatures, which was expected because it causes a reduction of both the activation- and ohmic losses. The low conductivity of YSZ at lower temperatures has already been mentioned in previous sections. An interesting aspect is to compare the increasing rate of the maximum power densities of ammonia and the hydrogen/nitrogen mixture. The former has clearly an exponential relationship to the temperature due to process of cracking ammonia. This can be seen in Fig 58 of the maximum power densities where the ammonia has a rather sluggish increase rate at first but goes rapidly faster after 800°C is passed. On the other hand, the rate of increment of the hydrogen/nitrogen mixture is steady from start to end, forming an almost linear line. This substantiates the importance of an active cracking process, as it greatly impacts the performance.

5.3.3 Pure Hydrogen - 600°C to 850°C

Hydrogen is the most basic and simple fuel in terms of fuel cell reaction and working principles. In this study is hydrogen acting as a reference to show the performance of an “ideal” fuel and was used to evaluate the performance of ammonia. In terms of shape and temperature dependency is the results like the previous scenario, but there is a slightly higher OCV due to the

increased partial pressure of hydrogen. The assumption of an increase of partial pressure is substantiated by the assumption of a constant total pressure of 1atm in the gas chambers, reasoned by the fact the cell is an open flange.

5.3.4 Comparison

Fig 54 to 56 presents a combined plot of I/V- and power density curves of the three fuels at 650°C, 750°C and 850°C. The first portion (until ~25mA/cm^2) is mainly due to activation loss, but the curve is eventually dominated by the ohmic losses, seen by the linear behaviour. From the plotted graphs it is seen that the maximum power density of hydrogen and hydrogen/nitrogen mixture is almost identical until 40mA/cm^2, where they slowly drift apart as the current increases. The size of the gap at a specific current density is maintained the same at all temperatures, indicating that the loss is not temperature dependent but is related to a changed inherent resistance or mass-transfer losses in the cell due to the dilution of nitrogen. Variances in the electrode polarisation can occur due to fuel being diluted by nitrogen but is difficult determine without performing EIS analysis. Unfortunate, this was not done due to issues with the EIS tester.

Ammonia on the other hand, or the process of cracking ammonia, is clearly benefitting from higher temperatures, and especially the plot of 850°C show the importance of an active cracking process to achieve comparable results to hydrogen. The maximum power density at 650°C and 750°C is approximate 7mW/cm^2 and 20mW/cm^2 and corresponds to just a little more than half of the values obtained by pure hydrogen and the hydrogen/nitrogen mixture at the same temperatures. This was expected due to the presence of steam from the aqueous ammonia solution, lowering the concentration of hydrogen in flow to the chamber. Similar results are also found in by G. Cinti et al.[13] in their study of a stack fuelled by diluted and pure ammonia. Nevertheless, as the temperature approaches 850°C the difference between ammonia and the two other scenarios are almost vanished. The first 100mA/cm^2 of the hydrogen/nitrogen mixture and ammonia solution are almost identical, but the nitrogen/hydrogen starts then to decrease relatively fast while the ammonia maintains its shape. It is known that pure ammonia gas can reach the same performance as hydrogen/nitrogen mixture, but it was expected some reduction due to the presence of steam from the aqueous solution. This is a topic that is not fully understood by the author. At the higher current densities is even the ammonia approaching the hydrogen.

The OCV of H_2 is marginally higher than the one of H_2/N_2 due to an increased hydrogen partial pressure. This is reasoned by looking at Nernst equation. Assuming a constant total pressure in the chamber of 1atm, this would result in a drop of hydrogen partial pressure by approximate ¼ due to the presence of nitrogen in the hydrogen/nitrogen scenario. However, the difference is not as significant as expected and can be due to a slightly increased total pressure maintaining the partial pressure to a great extent. This effect is more drastic when operating the cell with aqueous ammonia due to the presence of steam as mentioned in the previous section. The presence of steam as a significant impact of the OCV voltage because it both reduce the concentration of hydrogen in the fuel and push the reaction in the wrong direction. The effect can be seen in Fig 57 of the OCV voltages, showing a significantly reduction while operating with ammonia solution.

5.4 Modelling

It was developed a simple electrochemical model fitted to experimental data of the cell running with hydrogen at 750°C. There are many approaches capable to describe the happenings in a fuel cell and the approach used in this cell is explained in chapter 2.4 and 3.2. The purpose of the model is to act as a tool to estimate fuel cell parameters that can otherwise are difficult to obtain, such as exchange current, activation energy and polarization losses. The modelled polarization curve presented in Fig 61 fits significantly well to the exponential curve after some fitting of parameters. The figure show that activation losses by far is the most significant source of polarization losses, mainly caused by the cathode reaction. The slope at the final portion of the of the experimental and modelled curve match, indicating that the ohmic losses are somewhat accurate. The diffusion losses are as good as negligible, which is as expected due to reasoning previously mentioned.

The model was fitted by adjust the activation energy and pre-exponential coefficient of the anode and cathode until the curve matched the experimental curve. Parameters such as electrolyte conductivity, pore radius and tortuosity among other thing was taken from relevant papers that was presented in chapter 3.2 and maintained constant. It should be mentioned that many approaches and parameters values are found is literatures, meaning there is likely deviations between the modelled and real polarization losses. Nevertheless, the model fits very well with the experimental data and is probably giving a good estimation of the actual values. It therefore serves it purpose.

6 Conclusion

The objective of this thesis was to investigate if ammonia is a feasible fuel for SOFC systems. To answer this question was an experimental work of an Open Flange SOFC with a planar anode-supported single cell composed by a Ni/YSZ anode, YSZ electrolyte and LSM cathode tested. The cell was operated at temperatures between 600°C to 850°C with three variations of aqueous ammonia solutions (32wt%, 15.2wt% and 5.9wt%), pure hydrogen, and a simulation of pre-cracked ammonia. The experiment was conducted to analyse the effect of the endothermic cracking process and dilution of nitrogen and steam on the overall performance of the cell.

The experimental work was divided into two parts. First were three variations of ammonia solution evaluated at a constant temperature of 750°C to see the impact of partial pressure and mass flow of ammonia on the overall performance. The results showed maximum power densities at 45 mW/cm^2, 37.5 mW/cm^2, and 25 mW/cm^2 which were consistent with the expected reduction in partial pressure and mass flow of ammonia. In the second part 32wt% ammonia solution, pure hydrogen and a mixture of nitrogen and hydrogen was tested from 600°C to 850°C in steps of 50°C. The hydrogen/nitrogen obtained almost the same curve as hydrogen at 600°C but became slowly distanced at higher temperatures and current densities. Ammonia obtained approximate half the maximum power densities of hydrogen at all temperatures up to 800°C. Sluggish cracking process and the presence of steam from the aqueous solution was expected reasons to cause a reduced performance. Nonetheless, a big jump at 850°C resulted in a maximum power density higher than pre-crack ammonia, and very well comparable to hydrogen. It is known that the process of cracking ammonia favours higher temperatures, but it was expected some loss due to the presence of steam in the mass flow mixture. This is however a positive result, that could be taken to further investigation.

In additions, an electrochemical model of the SOFC operated with hydrogen was developed and fitted to experimentally obtained data as a method to estimate polarisation loss and fuel parameters that is otherwise difficult to obtain. The adjustable parameters were the activation energy and pre-exponential coefficients. The modelling curve matches the curve from the experiment and is assumed that the modulation parameters is accurate. Some deviation from the actual cell is likely due to numerous assumptions, but the model serves its purpose of estimating polarisation losses and exchange current densities.

Based on the results presented in this thesis, especially of ammonia at 850°C, it can be concluded that 32wt% aqueous ammonia solution is a feasible alternative of fuelling SOFC at temperatures above 800°C. The concentration is clearly affecting the performance and other experiment has showed great performance with pure ammonia at lower temperatures. Nonetheless, SOFC still needs to solve obstacles regarding its low durability and slow response time before it can be regarded a feasible option for power generating in maritime applications. It is therefore not expected to see ships powered by SOFC alone in the coming years, but more likely in combination with ICE or similar technologies.

7 Recommendations

This study was limited to the use of aqueous solutions due lab facilities unable to handle the associated toxicity of pure ammonia. It is under planning to install a system to supply pure ammonia gas to operate the cell. This would allow more in-depth and realistic data to be obtained.

It is still done research to discover whether ammonia causes a long-term degradation of the cell. Therefore, a long-term experiment of the cell operated with ammonia at a constant current or voltage would be interesting.

The cell used in this experiment was pre-made with some uncertainties about composition and operating hours prior to this project. Creating or buying cell with the known composition would further substantiate the experimental results.

Most of the issues of SOFC is improved or solved at lower temperatures. This would however require a more advanced catalyst and electrolyte than the currently state-of-the-art materials. Develop and test alternative materials of cathode, anode and electrolyte is a

8 References

[1] F. O. R. Business, "Adapt to Survive : Business transformation in a time of uncertainty," 2021.

[2] IMO, "Fourth IMO GHG Study 2020 – Final report," Jul. 2020.

[3] IMO, "Adoption of the Initial IMO Strategy on Reduction of GHG Emissions From Ships and Existing Imo Activity Related To Reducing Ghg Emissions in the Shipping Sector," *Mepc 72*, p. 27, 2018.

[4] K. Y. K. & T.-H. J. Hyungju Kim, "A study on the necessity of integrated evaluation of alternative marine fuels, Journal of International Maritime Safety, Environmental Affairs, and Shipping," *J. Int. Marit. Safety, Environ. Aff. Shipp.*, vol. 4, no. 2, p. 7, 2020, doi: 10.1080/25725084.2020.1779426.

[5] DNV GL, "Energy Transition Outlook 2020: Maritime Forecast To 2050," 2020.

[6] DNV GL, "Assessment of Selected Alternative Fuels and Technologies," 2019.

[7] The Royal Society, "Ammonia: zero-carbon fertiliser, fuel and energy store. Policy Briefing." p. 40, 2020.

[8] P. T. Moseley, *Fuel Cell Systems Explained*, vol. 93, no. 1–2. 2001.

[9] J. B. G. Kevin Huang, *Solid oxide fuel cell technology - Principles, performance and operations*. Woodhead Publishing Limited, 2009.

[10] Q. Ma, R. R. Peng, L. Tian, and G. Meng, "Direct utilization of ammonia in intermediate-temperature solid oxide fuel cells," *Electrochem. commun.*, vol. 8, no. 11, pp. 1791–1795, 2006, doi: 10.1016/j.elecom.2006.08.012.

[11] A. Wojcik, H. Middleton, I. Damopoulos, and J. Van Herle, "Ammonia as a fuel in solid oxide fuel cells," *J. Power Sources*, vol. 118, no. 1–2, pp. 342–348, 2003, doi: 10.1016/S0378-7753(03)00083-1.

[12] Y. Wang *et al.*, "Low–Temperature Ammonia Decomposition Catalysts for Direct Ammonia Solid Oxide Fuel Cells," *J. Electrochem. Soc.*, vol. 167, no. 6, p. 064501, 2020, doi: 10.1149/1945-7111/ab7b5b.

[13] G. Cinti, G. Discepoli, E. Sisani, and U. Desideri, "SOFC operating with ammonia: Stack test and system analysis," *Int. J. Hydrogen Energy*, vol. 41, no. 31, pp. 13583–13590, 2016, doi: 10.1016/j.ijhydene.2016.06.070.

[14] H. Council and McKinsey&Company, "Hydrogen Insights: A perspective on hydrogen investment, market development and cost competitiveness," 2021.

[15] M. Jaganmohan, "Share of global hydrogen production 2020, by type," 2021. https://www.statista.com/statistics/1200503/global-hydrogen-production-share-by-type/.

[16] K. H. R. Rouwenhorst, P. M. Krzywda, N. E. Benes, G. Mul, and L. Lefferts, *Chapter 4 - Ammonia Production Technologies*. Elsevier Inc., 2021.

[17] C. Benjaminsen, "This is what you need to know about CCS - Carbon Capture and Storage," 2019. https://www.sintef.no/en/latest-news/2019/this-is-what-you-need-to-know-about-ccs-carbon-capture-and-storage/.

[18] Bellona, "Hydrogen from methane reforming + CCS," 2020. https://www.frompollutiontosolution.org/hydrogen-from-smr-and-ccs.

[19] M. Bui *et al.*, "Carbon capture and storage (CCS): The way forward," *Energy Environ. Sci.*, vol. 11, no. 5, pp. 1062–1176, 2018, doi: 10.1039/c7ee02342a.

[20] N. de Vries, "REPORT (THESIS) - Safe and effective application of ammonia as a marine fuel," Delft University of Technology, 2019.

[21] E. Baniasadi and I. Dincer, "Energy and exergy analyses of a combined ammonia-fed solid oxide fuel cell system for vehicular applications," *Int. J. Hydrogen Energy*, vol. 36, no. 17, pp. 11128–11136, 2011, doi: 10.1016/j.ijhydene.2011.04.234.

[22] E. Wachsman, T. Ishihara, and J. Kilner, "Low-temperature solid-oxide fuel cells," *MRS*

Bull., vol. 39, no. 9, pp. 773–779, 2014, doi: 10.1557/mrs.2014.192.
[23] G. Meng, C. Jiang, J. Ma, Q. Ma, and X. Liu, "Comparative study on the performance of a SDC-based SOFC fueled by ammonia and hydrogen," *J. Power Sources*, vol. 173, no. 1, pp. 189–193, 2007, doi: 10.1016/j.jpowsour.2007.05.002.
[24] H. Shi, C. Su, R. Ran, J. Cao, and Z. Shao, "Electrolyte materials for intermediate-temperature solid oxide fuel cells," *Prog. Nat. Sci. Mater. Int.*, vol. 30, no. 6, pp. 764–774, 2020, doi: 10.1016/j.pnsc.2020.09.003.
[25] B. Shri Prakash, S. Senthil Kumar, and S. T. Aruna, "Properties and development of Ni/YSZ as an anode material in solid oxide fuel cell: A review," *Renew. Sustain. Energy Rev.*, vol. 36, pp. 149–179, 2014, doi: 10.1016/j.rser.2014.04.043.
[26] M. Cimenti and J. M. Hill, "Direct utilization of liquid fuels in SOFC for portable applications: Challenges for the selection of alternative anodes," *Energies*, vol. 2, no. 2, pp. 377–410, 2009, doi: 10.3390/en20200377.
[27] J. Liu and S. A. Barnett, "Thin yttrium-stabilized zirconia electrolyte solid oxide fuel cells by centrifugal casting," *J. Am. Ceram. Soc.*, vol. 85, no. 12, pp. 3096–3098, 2002, doi: 10.1111/j.1151-2916.2002.tb00588.x.
[28] A. Fuerte, R. X. Valenzuela, M. J. Escudero, and L. Daza, "Ammonia as efficient fuel for SOFC," *J. Power Sources*, vol. 192, no. 1, pp. 170–174, 2009, doi: 10.1016/j.jpowsour.2008.11.037.
[29] GloMEEP Project Coordination Unit International Maritime Organization and S. and T. (IMarEST) Institute of Marine Engineering, "Ship Emissions Toolkit - Guide No.1: Rapid assessment of ship emission in the national context," 2018.
[30] A. Afif, N. Radenahmad, Q. Cheok, S. Shams, J. H. Kim, and A. K. Azad, "Ammonia-fed fuel cells: A comprehensive review," *Renew. Sustain. Energy Rev.*, vol. 60, pp. 822–835, 2016, doi: 10.1016/j.rser.2016.01.120.
[31] United State Department of Energy, "Status of the Solid Oxide Fuel Cell Program," no. August, 2019.
[32] Y. Lin *et al.*, "Proton-conducting fuel cells operating on hydrogen, ammonia and hydrazine at intermediate temperatures," *Int. J. Hydrogen Energy*, vol. 35, no. 7, pp. 2637–2642, 2010, doi: 10.1016/j.ijhydene.2009.04.019.
[33] L. Zhang and W. Yang, "Direct ammonia solid oxide fuel cell based on thin proton-conducting electrolyte," *J. Power Sources*, vol. 179, no. 1, pp. 92–95, 2008, doi: 10.1016/j.jpowsour.2007.12.061.
[34] M. Ni, D. Y. C. Leung, and M. K. H. Leung, "Mathematical modeling of ammonia-fed solid oxide fuel cells with different electrolytes," *Int. J. Hydrogen Energy*, vol. 33, no. 20, pp. 5765–5772, 2008, doi: 10.1016/j.ijhydene.2008.07.021.
[35] S. H. Chan, K. A. Khor, and Z. T. Xia, "Complete polarization model of a solid oxide fuel cell and its sensitivity to the change of cell component thickness," *J. Power Sources*, vol. 93, no. 1–2, pp. 130–140, 2001, doi: 10.1016/S0378-7753(00)00556-5.
[36] B. Todd and J. B. Young, "Thermodynamic and transport properties of gases for use in solid oxide fuel cell modelling," *J. Power Sources*, vol. 110, no. 1, pp. 186–200, 2002, doi: 10.1016/S0378-7753(02)00277-X.
[37] L. van Biert, M. Godjevac, K. Visser, and P. V. Aravind, "Dynamic modelling of a direct internal reforming solid oxide fuel cell stack based on single cell experiments," *Appl. Energy*, vol. 250, no. March, pp. 976–990, 2019, doi: 10.1016/j.apenergy.2019.05.053.
[38] M. L. Williams, *CRC Handbook of Chemistry and Physics, 76th edition*, 84th ed., vol. 53, no. 7. CRC Press, 1996.
[39] C. Borgnakke; and R. E. Sonntag, *Fundamentals of Thermodynamics*, 7th editio., vol. 110, no. 9. John Wiley & sons, inc, 2009.
[40] L. Theodore, F. Ricci, and T. Van Vliet, *Thermodynamics for the Practicing Engineer*. New Jersey: John Wiley & sons, 2009.
[41] B. Pedersen, "aktiveringsenergy," 2018. .
[42] D. A. Noren and M. A. Hoffman, "Clarifying the Butler-Volmer equation and related

approximations for calculating activation losses in solid oxide fuel cell models," *J. Power Sources*, vol. 152, no. 1–2, pp. 175–181, 2005, doi: 10.1016/j.jpowsour.2005.03.174.

[43] M. Ni, M. K. H. Leung, and D. Y. C. Leung, "Parametric study of solid oxide fuel cell performance," *Energy Convers. Manag.*, vol. 48, no. 5, pp. 1525–1535, 2007, doi: 10.1016/j.enconman.2006.11.016.

[44] A. Leonide, "SOFC Modelling and Parameter Identification by means of Impedance Spectroscopy," 2010.

[45] S. Khan, S. M. A. Rizvi, and Shabana Urooj, "Equivalent Circuit Modellingusing Electrochemical Impedance Spectroscopy for Different Materials of SOFC," Bharati Vidyapeeth, New Delhi as the Organizer of INDIACom - 2016, 2016.

[46] Q. A. Huang, R. Hui, B. Wang, and J. Zhang, "A review of AC impedance modeling and validation in SOFC diagnosis," *Electrochim. Acta*, vol. 52, no. 28, pp. 8144–8164, 2007, doi: 10.1016/j.electacta.2007.05.071.

[47] D. Das and Submitted, "Electrochemical Degradation , Kinetics & Performance Studies of Solid Oxide Fuel Cells," no. May, 2016.

[48] U. S. E. P. A. (EPA), "Human-Health-Risk-Assessment @ Www.Epa.Gov," 2021. http://www.epa.gov/risk/human-health-risk-assessment (accessed Mar. 18, 2021).

[49] G. Cinti, U. Desideri, D. Penchini, and G. Discepoli, "Experimental analysis of SOFC fuelled by ammonia," *Fuel Cells*, vol. 14, no. 2, pp. 221–230, 2014, doi: 10.1002/fuce.201300276.

A – Appendix

```
close all;
clear;

%***********EXPERIMENTAL DATA*********************
%Importing results from Hydrogen/Nitrogen experiment
Data = readtable('H2TempPlot.xlsx', 'Range',
'A2:AD25');
column_name = {'T_600' 'T_650' 'T_700' 'T_750'
'T_800' 'T_850'};
%Extracting Cell Voltage to its own table
Voltage =
table(Data.Voltage,Data.Voltage_1,Data.Voltage_2,
Data.Voltage_3, Data.Voltage_4, Data.Voltage_5);
Voltage.Properties.VariableNames = column_name;
%Extracting Current density to its own table [
A_dens =
table(Data.Current_1,Data.Current_3,Data.Current_5,
Data.Current_7, Data.Current_9, Data.Current_11);
A_dens.Properties.VariableNames = column_name;
A_dens.Variables = ((100*100)/1000)*A_dens.Variables;
%[A/m2]
%***********MATHEMATICAL MODEL*********************
%Constants
pore_r = 5e-7;
porosity = 0.3;
tort = 6;
p_H2_s = 0.97;
p_H2O_s = 0.03;
p_O2_s = 0.21;
p_N2_s = 0.79;
R = 8.314;          %J/mol K
F = 96487;          %C/Mol e-
k = 1.38064e-23;    %boltzmann constant [m2kg/s2K]
z = 2;              %number of free electrons pr
reaction
TC = 750;               %Degree C;
T = 273.15+TC;          %degree C to K
%Molar Mass [kg/mol]
M_H2 = 2.016;       %[kg/mol]
M_O2 = 31.999;      %[kg/mol]
```

```
M_H2O = 18.015;      %[kg/mol]
M_N2 = 28.015;       %[kg/mol]
%Fuller et al. special diffusion volume
V_H2 = 6.12e-6;     %[m3/mol]
V_O2 = 16.3e-6;     %[m3/mol]
V_H2O = 13.1e-6;    %[m3/mol]
V_N2 = 18.5e-6;    %[m3/mol]
%Cell paramteres
r = 3.5/2/100;           %radius single cell [m]
A = pi*r^2;              %area single cell [m2]
alpha = 0.5;             %Transfer coefficient, equal
for anode and cathode
    %anode
    E_act_a = 145e3;         %Activation energy anode
    cond_a= 80e3;            %Conductivity anode
[ohm^-1 m^-r1]
    cond_a= 30.3e3;            %Conductivity anode
[ohm^-1 m^-r1]
    b_a = 6.6e11;            %Pre-Exponential
coefficient anode
    t_a = 200e-6;            %[m] - thickness of anode
    D_a = 3.66e-5;           %[m2/s] Molecular diff.
coef.
    %electrolyte
%     cond_el= 33.4e3*exp((-10.3e3)/T);
%Conductivity electrolyte [ohm^-1 m^-1]
    cond_el= 33.4e3*exp((-11e3)/T);    %Conductivity
electrolyte [ohm^-1 m^-1]
    t_el = 20e-6;            %[m] -thickness of
electrolyte
    %Cathode
    E_act_c = 153e3;         %Activation energy
cathode
    cond_c= 12.9e3;           %Conductivity cathode
[ohm^-1 m^-1]
%     b_c = 2.35e11;           %Pre-Exponential
coefficient cathode
    b_c = 1.45e11;           %Pre-Exponential
coefficient cathode
    t_c = 20e-6;             %[m] - thicnkess cathode
    D_c = 1.37e-5;           %[m2/s] Molecular
diff.coef.
%Pressure and molar fraction
```

```
p_tot = 1;                  %Total Pressure
p0 = 1;                     %Standard pressure
m_H2 = 1;                   %Mole of H1
m_O2 = 0.5;                 %Moles of Oxygen
m_H2O = 1;                  %Moles of water
m_tot = m_H2+m_O2+m_H2O;    %Total number of moles
%Molar fractions
x_H2 = m_H2/m_tot;          %Molar fraction Hydrogen
x_O2 = m_O2/m_tot;          %Molar fraction Oxygen
x_H2O = m_H2O/m_tot;        %Molar fraction Water
%Partial pressures
P_H2 = 0.97;          %Partial pressure of hydrogen,
approximated to 1
P_O2 = 0.21;          %Partial pressure of air
P_H2O = 0.03;         %Partial pressure of water

%calculating OCV -> nerst equation as a function of
temp and pressure
E0_rev = -(-190.31e3/(z*F));    %Gibbs Free Energy at
750 degC (from excel file)
E_rev = E0_rev-
((R*T/(z*F))*log(P_H2O/(P_H2*P_O2^0.5)));    %Nernst
Equation, Estimated partial pressures
    %First calculating values of i0 at anode and
cathode
    i0_a = (R*T/(z*F))*b_a*exp(-E_act_a/(R*T));
%Exchange current Anode
    i0_c = (R*T/(z*F))*b_c*exp(-E_act_c/(R*T));
%Exchange current Cathode

Counter = 1;    %To store data in tables
c = 0;          %Initial current value
c_end = 1800;   %[mA/cm]
cdt = 5;        %Current increase for each
integration
while c <= c_end     %[mA/cm2]
    %Activation polarisation
    V_act_a = (R*T/(alpha*F))*asinh(c/(2*i0_a));
    V_act_c = (R*T/(alpha*F))*asinh(c/(2*i0_c));
    V_act = V_act_a+V_act_c;
    %Ohmis polarisation
    R_cell = t_a/cond_a + t_el/cond_el + t_c/cond_c;
%[Ohm m2]
```

```
    V_ohm = R_cell*c*(10000/1000);       %[ohm
m2]*[A/m2]
    %Diffusion losses
    M_H2_H2O = 2*((1/M_H2)+(1/M_H2O))^-1;
%Hydrogen-Steam
    M_H2_O2 = 2*((1/M_H2)+(1/M_O2))^-1;
%Hydrogen-Oxygen
    M_O2_H2O = 2*((1/M_O2)+(1/M_H2O))^-1;
%Oxygen-steam
    M_O2_N2 = 2*((1/M_O2)+(1/M_N2))^-1;
%Oxygen_Nitrogen
    %Binary diffusion coefficient [m2/s]
    D_H2_H2O =
(0.00143*T^1.75)/(p_tot*(M_H2_H2O^0.5)*(V_H2^(1/3)+V_
H2O^(1/3))^2);      %Hydrogen-Steam
    D_H2_O2 =
(0.00143*T^1.75)/(p_tot*(M_H2_O2^0.5)*(V_H2^(1/3)+V_O
2^(1/3))^2);         %Hydrogen-Oxygen
    D_O2_H2O =
(0.00143*T^1.75)/(p_tot*(M_O2_H2O^0.5)*(V_O2^(1/3)+V_
H2O^(1/3))^2);      %Oxygen-Steam
    D_O2_N2 =
(0.00143*T^1.75)/(p_tot*(M_O2_N2^0.5)*(V_O2^(1/3)+V_N
2^(1/3))^2);         %Oxygen-nitrogen
    %Knudsen diffusion coefficient
    Dk_H2 = 97*pore_r*sqrt(T/M_H2);          %Hydrogen
    Dk_H2O = 97*pore_r*sqrt(T/M_H2O);        %Steam
    Dk_O2 = 97*pore_r*sqrt(T/M_O2);          %Oxygen
    Dk_N2 = 97*pore_r*sqrt(T/M_N2);          %Nitrogen
    %Molecular diffuson coefficient
    Dg_H2 = (1-p_H2_s)/((p_H2O_s/D_H2_H2O));
%Hydrogen
    Dg_H2O = (1-p_H2O_s)/((p_H2_s/D_H2_H2O));
%Steam
    Dg_O2 = (1-p_O2_s)/(p_N2_s/D_O2_N2);
%Oxygen
    Dg_N2 = (1-p_N2_s)/((p_O2_s/D_O2_N2));
%Nitrogen
    %Effective diffusion coefficient
    Deff_H2 = porosity/tort*((1/Dg_H2)+(1/Dk_H2));
%Hydrogen
    Deff_H2O = porosity/tort*((1/Dg_H2O)+(1/Dk_H2O));
%Steam
```

```
    Deff_O2 = porosity/tort*((1/Dg_O2)+(1/Dk_O2));
%Oxygen
    Deff_N2 = porosity/tort*((1/Dg_N2)+(1/Dk_N2));
%Nitrogen
    Deff_a = p_H2_s*Deff_H2+p_H2O_s*Deff_H2O;
%Anode
    Deff_c = p_O2_s*Deff_H2+p_N2_s*Deff_N2;
%Cathode

    %Calculate partial pressure at TBL
    p_H2_TBL = p_H2_s-
(R*T*t_a)/(2*F*Deff_a)*c*(10000/1000);
%Hydrogen Partial pressure TBL
    p_H2O_TBL =
p_H2O_s+(R*T*t_a)/(2*F*Deff_a)*c*(10000/1000);
%Steam partial pressure TBL
    p_O2_TBL = p_tot-(p_tot-
p_O2_s)*exp((R*T*t_c*c*(10000/1000))/(4*F*Deff_c*p_to
t));
    %Concentration loss
    V_Conc =
(R*T/(2*F))*log(p_H2O_TBL*p_H2_s/(p_H2O_s*p_H2_TBL))+
(R*T/(4*F))*log(p_O2_s/p_O2_TBL);

    %Store data
    V_Cell(Counter) = E_rev-V_act_a-V_act_c-V_ohm-
V_Conc;
    H2_TBL(Counter) = p_H2_TBL;
    H2O_TBL(Counter) = p_H2O_TBL;
    O2_TBL(Counter) = p_O2_TBL;
    Current(Counter) = c;
    R_loss(Counter) = V_ohm;
    Act_a_loss(Counter) = V_act_a;
    Act_c_loss(Counter) = V_act_c;
    Conc_loss(Counter) = V_Conc;
    Counter = Counter + 1;
    c = c+cdt;
end

figure1 = figure('color', [1,1,1]);
hdlp1 = plot(Current, V_Cell, 'r');
grid
hold on
```

```
hdlp2 = plot(A_dens.T_750, Voltage.T_750, 'b',
'Linewidth', 1.5);
hdlp3 = plot(Current, Act_a_loss, '--c', 'Linewidth',
1.5);
hdlp4 = plot(Current, Act_c_loss, '-.m', 'Linewidth',
1.5);
hdlp5 = plot(Current, R_loss, 'g', 'Linewidth', 1.5);
hdlp6 = plot(Current, Conc_loss, ':k', 'Linewidth',
1.5);
%Figure make-up
axis([0 1800 0 1.12]);
ax = gca;
ax.FontSize =24;
xticks(0:200:1800);
yticks(0:0.05:1.2);
legend('Modelling', 'Experimental', 'Anode Activation
loss','Cathode Activation loss', 'ohmic
loss','Diffusion Losses','Fontsize', 28);
title('Modelling of SOFC fuelled by Hydrogen at 750
^{o}C ', 'Fontsize', 32);
xlabel('Current [mA/cm^2]','Fontsize', 28);
ylabel('Cell Voltage [V]','Fontsize', 28);
box on
```